Potential of remote sensing of cirrus optical thickness by airborne spectral radiance measurements in different sideward viewing anglesand nadir geometry

Kevin Wolf[1], André Ehrlich[1], Tilman Hüneke[2], Klaus Pfeilsticker[2], Frank Werner[1,3], Martin Wirth[4], and Manfred Wendisch[1]

[1]Leipzig Institute for Meteorology, University of Leipzig, Leipzig, Germany

[2]Institute of Environmental Physics, University of Heidelberg, Heidelberg, Germany

[3]now at Joint Center for Earth Systems Technology, University of Maryland, Baltimore, MD, USA

[4]Institute of Atmospheric Physics, German Aerospace Center, Oberpfaffenhofen, Germany

Correspondence to: K. Wolf (kevin.wolf@uni-leipzig.de)

Abstract. Spectral radiance measurements from collected in nadir and sideward viewing directions by two airborne passive solar remote sensing instruments, the Spectral Modular Airborne Radiation measurement sysTem (SMART) and the Differential Optical Absorption Spectrometer (mini-DOAS), are used to compare the remote sensing results of cirrus optical thickness τin nadir and off-nadir geometry. The comparison is based on a sensitivity study using radiative transfer simulations and on measurements during (RTS) and on data obtained during three airborne field campaigns: the North Atlantic Rainfall VALidation (NARVAL) mission, the Mid-Latitude Cirrus Experiment (ML-CIRRUS) and the Aerosol, Cloud, Precipitation, and Radiation Interactions and Dynamics of Convective Cloud Systems (ACRIDICON) campaign. Radiative transfer simulations are used to quantify the sensitivity of measured upward radiance I with respect to cirrus optical thickness τ, ice crystal effective radius r_{eff}, viewing angle of the sensor θ_{L}, θ_{V}, spectral surface albedo α, and ice crystal shape. From the calculations it is concluded that off-nadir measurements sideward viewing measurements are generally suited better than radiances data from nadir direction to retrieve τ of optically thin cirrus, especially at wavelengths larger than λ = 900 nmsignificantly improve the ability to measure clouds of low optical thickness. Using sideward instead of nadir-directed spectral radiance measurements significantly improves the sensitivity and accuracy to retrieve τ in particular for optically thin cirrus of $\tau \leq 2$.

The comparison of nadir and off-nadir retrievals of τ from based on nadir and sideward viewing radiance measurements from SMART, mini-DOAS , SMARTand independent estimates by the Water Vapour of τ from an additional active remote sensing instrument, the Water Vapor Lidar Experiment in Space (WALES), show general agreement within the range of measurement uncertainties. For the selected example case a mean optical thickness a mean τ of 0.54 ± 0.2 is derived by SMARTfrom SMART, and 0.49 ± 0.2 by mini-DOAS nadir channels, while WALES obtained a mean value of 0.32 at 532 nm $\tau = 0.32 \pm 0.02$ at 532 nm wavelength respectively. The mean of τ derived from the scanning sideward viewing mini-DOAS channels is 0.260.26 $\pm$ 0.2. For the few simultaneous measurements, the scanning mini-DOAS sideward channel measurements systematically underestimate (- 17.6 %) the nadir observations from SMART and mini-DOAS, most likely due to the different probed scenes. The different values of τ derived by SMART, . The agreement between mini-DOAS and WALES can

~~be potentially linked to spatial averages, ice crystal shape and the measurement strategies. The agreement of the simulations and retrievals indicate that off-nadir measurements are generally suited better to retrieve~~ sideard viewing channels and WALES is better, showing the advantage of using sideward viewing measurements for cloud remote sensing for $\tau \leq 1$. Therefore, we suggest sideward viewing measurements for retrievals of τ of thin ~~clouds.~~ cirrus because of the significantly enhanced capability of sideward viewing compared to nadir measurements.

1 Introduction

The impact of cirrus on the atmospheric radiative energy budget and the Earth's climate system is uncertain (IPCC, 2013), which is partly due to the limited knowledge about the formation and development of cirrus (Sausen et al., 2005). Until now it is not sufficiently quantified to what fraction homogeneous or heterogeneous ice nucleation contributes to the cirrus formation (Cziczo et al., 2013). As a result, the evolution of the cirrus microphysical properties during ~~the~~ its life-cycle ~~of the cirrus~~ is insufficiently represented in climate models (IPCC, 2013). Further ~~the globally averaged~~ more, the influence of cirrus on the Earth's radiation budget is highly variable because it strongly depends on their microphysical properties such as ice crystal number, size and shape ~~(Zhang et al., 1999; Wendisch et al., 2005, 2007). Additionally, the radiative effects of different ice crystal sizes and shapes are not well quantified (Chen et al., 2000; Yang et al., 2012).Another problem in estimating the impact of cirrus on the Earth's energy budget is the presence of~~ (Zhang et al., 1999; Chen et al., 2000; Wendisch et al., 2005, 2007; Yang et al., 2012). In particular, optically thin cirrus ($\tau \leq 0.03$), so called sub-visible cirrus (SVC), ~~which~~ is difficult to observe and not well represented in ~~the~~ General Circulation Models ~~(GCM) (Wiensz et al., 2013). Despite the fact that SVC are optically thin ($\tau < 0.03$), they~~ (Wiensz et al., 2013). Sub-visible cirrus may extend over large areas (Davis et al., 2010). Therefore, their influence on the energy budget of the Earth can probably not be neglected. Lee et al. (2009) estimated the annually and globally averaged radiative forcing of SVC with ~~$+1\,\mathrm{W\,m^{-2}}$~~ $+1\,\mathrm{W\,m^{-2}}$ (warming effect), while ~~local forcings~~ the local forcing might be significantly higher. Especially, the location and time where SVC occur determine their radiative effects. Whether SVC heat or cool the atmosphere depends on surface albedo α, solar zenith angle θ_0 and cirrus optical thickness τ (Fu and Liou, 1993). In general SVC and cirrus have a heating effect at the top-of-atmosphere (TOA) since the reduction of outgoing infrared radiation usually dominates the cooling effect due to reflection of solar radiation (McFarquhar et al., 2000; Comstock et al., 2002; Davis et al., 2010).

In order to quantify ~~better the uncertainties related to SVC,~~ the microphysical and optical properties of SVC, which are needed to determine their radiative effects, more observations of ~~SVC appear worthwhile. Several~~ this cloud type are required. As a consequence, several satellite missions and field studies were performed in the past, e.g., by Wang et al. (1996), Winker and Trepte (1998), Sassen et al. (2009), and Jensen et al. (2015) to establish a reliable data base on SVC. Airborne in-situ measurements by ~~e. g., Lampert et al. (2009)~~Lampert et al. (2009), Davis et al. (2010), Froyd et al. (2010), and Frey et al. (2011) were utilized to determine ice crystal size and shape of ~~SVCs~~SVC. Optical and microphysical parameters derived from these measurements are used in radiative transfer simulation (RTS) and numerical weather prediction and climate modelling (Kärcher, 2002).

Despite these efforts, in-situ observations of SVC are still ~~limited~~ scarce and partly accidental due to the challenge of locating SVC~~, e. g.~~. Lampert et al. (2009) sampled an Arctic SVC after it was detected by an airborne lidar. Airborne campaigns dedicated to visible cirrus, e.g., Contrail, volcanoe and Cirrus Experiment (CONCERT, Voigt et al. (2010)), Mid-Latitude Cirrus (ML-CIRRUS, Voigt et al. (2016)) and tropical cirrus sampled during the Airborne Tropical TRopopause EXperiment (ATTREX) are more frequent (Delanoe et al., 2013; Ehret et al., 2014; Gross et al., 2015; Jensen et al., 2015) and occasionally include observations of SVC. Further international airborne missions like the Tropical Composition, Cloud and Climate Coupling (TC4) (Toon et al., 2010) and the Cirrus Regional Study of Tropical Anvils and Cirrus Layers - Florida Area Cirrus

Experiment (CRYSTAL-FACE) mission were conducted trying to fill the knowledge gap about the formation process and physical properties of tropical cirrus (Jensen et al., 2015).

While satellite observations are suited to study the global coverage of cirrus, their spatial and temporal resolution is ~~inherently limited~~ still limited and can not resolve the high spatial variability of cirrus. As a consequence ~~of the high spatial variation of the relevant parameters the influence of different microphysical parameters~~the 3 dimensional (3-D) radiative effects of different cirrus properties, e.g., ~~ice crystal shape, on the radiative budget of the Earth~~ τ, ice crystal size and shape, can not be studied using ~~such coarse resolution remote sensing instrumentation. This emphasizes the need for in-situ measurements providing a large temporal and spatial resolution . As a result, airborne remote sensing is required to bridge local in-situ and global satellite observations~~the coarse resolution of satellite remote sensing. Ground-based lidar and radar remote sensing can provide a high temporal resolution but are limited to a fixed location. In-situ airborne measurements can provide cirrus properties with both.

For passive remote sensing of cirrus nadir and ~~off-nadir~~ sideward viewing observations are available. For nadir ~~observations the cirrus optical thickness~~ measurements τ and the effective radius r_{eff} of ~~water clouds~~ liquid water droplets can be retrieved by the bi-spectral reflectivity method after Twomey and Seton (1980) and Nakajima and King (1990). Ou et al. (1993), Rolland et al. (2000), and King et al. (2004) adapted this method for ice clouds by introducing some modifications with regard to the thermodynamic phase and crystal shape of the ice particles. Especially due to the crystal shape and low values of τ cirrus retrievals lead to ~~higher uncertainties as compared to~~ additional uncertainties compared to liquid water clouds (Eichler et al., 2009; Fricke et al., 2014).

For low τ, the reflected radiation is dominated by the surface reflection below the cirrus. This may introduce a bias in the retrieval of τ of up to 30 % when ~~the surface albedo~~ α is not accurately known or inhomogeneous (Fricke et al., 2014). ~~However, even over dark~~ Over dark ocean surfaces the radiance I reflected by the cirrus might be weak and can be in the same order of magnitude as Rayleigh scattering in the atmosphere. In addition, inhomogeneities of cirrus lead to ~~three-dimensional~~ (3-D) radiative effects, which may cause a bias in the one-dimensional (1-D) radiative transfer simulations (Eichler et al., 2009). Incorrectly assumed ice crystal shapes also contribute to the retrieval uncertainty. Eichler et al. (2009) investigated the influence of ice crystal shape on derived τ and r_{eff}. Evaluating a case study, they concluded that different shapes can lead to relative differences in τ of up to 70 %. In ~~summary~~a worst scenario, all these effects ~~can~~ render retrievals of τ to become rather inaccurate~~and impossible~~. However, observations in sideward or limb viewing direction and improvements of retrieval techniques may overcome these limitations.

~~Off-nadir~~ Limb measurements of SVC and cirrus were first introduced and utilized for satellite measurements by Woodbury and McCormick (1986). Since then, several applications based on this method were developed and are ~~not~~ routinely be used~~in~~ , e.g. for trace gas measurements ~~(Wang et al., 1996; Bourassa et al., 2005; Fu et al., 2007)~~(Abrams et al., 1996; Wang et al., 1996; Many trace gas retrievals from aircraft, balloons and satellites are based on ultraviolet (UV)/ visible (VIS)/ near infrared (~~SWIR) off-nadir~~ IR) sideward viewing measurements in combination with differential optical absorption spectroscopy (DOAS), e.g. performed by Platt and Stutz (2008). Compared to nadir observations, radiance measurements in ~~off-nadir~~ limb or sideward viewing geometry are supposed to be ~~highly~~ more sensitive to optical thin clouds due to their observation geometry. One recent study was accomplished by Wiensz et al. (2013) who used satellite ~~off-nadir~~ limb measurements especially for SVC investigation in the tropical tropopause layer~~(TTL)~~. This data source improved SVC observations with respect to cloud climatology and

microphysics.

In the present study, retrievals of τ ~~based~~ base on simultaneous airborne nadir and ~~off-nadir~~ sideward viewing observations of cirrus and are compared to elaborate the potential of ~~off-nadir~~ sideward viewing measurements to derive optical parameters of SVC and optically thin cirrus. This includes a sensitivity study using ~~radiative transfer simulations (RTS)~~ RTS presented in Section 2 and measurements collected on board of the High Altitude and LOng range research aircraft (HALO) of the German Aerospace Center (DLR). With a maximum ceiling altitude of around 15 km ~~the HALO aircraft is feasible~~ HALO is capable to operate in and above SVC and cirrus in mid-latitudes and polar regions for in-situ measurements. The airborne observations are obtained with the Spectral Modular Airborne Radiation measurement sysTem (SMART) (Wendisch et al., 2001) and the Differential Optical Absorption Spectrometer (mini-DOAS) ~~(Hüneke, 2011)~~ (Hüneke et al., 2017) both assembled on HALO. The instrumentation is introduced in Section 3. Observations from four campaigns, the Mid Latitude Cirrus experiment (ML-CIRRUS), the Next-generation Aircraft Remote sensing for Validation Studies (NARVAL North and South), and the Aerosol, Cloud, Precipitation, and Radiation Interactions and Dynamics of Convective Cloud Systems (ACRIDICON-CHUVA) (Wendisch et al., 2016) are used to cross-calibrate the two individual instruments in terms of absolute radiance I as presented in Section 4. In Section 5 an iterative retrieval of τ is introduced. Utilizing the cross-calibrations together with nadir and ~~off-nadir~~ sideward viewing measurements of upward I, the retrieved results are presented and compared to reference measurements of τ ~~.~~ to emphasize the advantages of sideward viewing observations. Section 6 concludes the study.

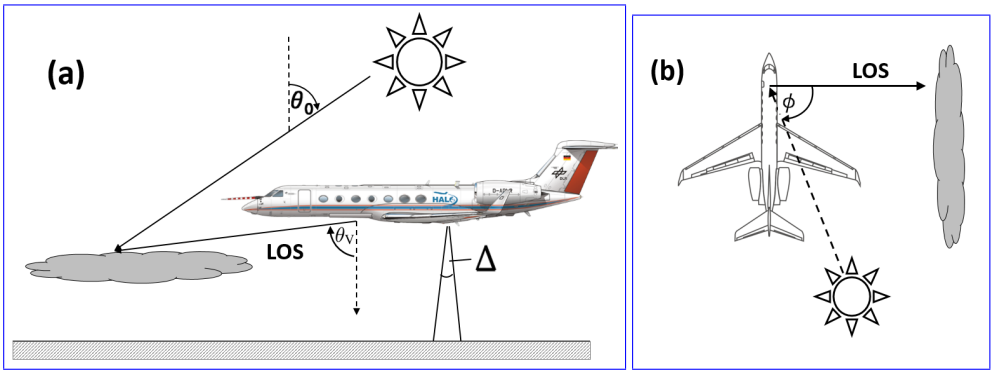

Figure 1. Illustration of the measurement geometry. (a) shows the side view with solar zenith angle θ_0 and the viewing angle ~~θ_L~~θ_V. The opening angle of the nadir looking radiance sensor of SMART is indicated by Δ. Top view (b) shows the definition of the relative solar azimuth angle ϕ between the line-of-sight (LOS) and the Sun.

2 Sensitivity of ~~remote sensing~~ upward radiance measurements in nadir and ~~off-nadir~~ sideward viewing directions

Radiative transfer simulations ~~(RTS) are first~~ are performed to investigate the sensitivity of solar radiance measurements in nadir and ~~off-nadir geometry for sub-visible and visible~~ sideward viewing geometry for SVC and thin cirrus. In this way the potential of ~~off-nadir~~ sideward viewing versus nadir observations for cirrus cloud parameter detection ~~(τ and r_{eff})~~ is examined.

Figure 1 illustrates the ~~definition of the~~ measurement geometry. The solar zenith angle ~~(SZA)~~ θ_0 is the angle between zenith and the Sun. The viewing angle ~~θ_L describes~~ θ_V represents the angle of the sensor ~~orientation~~ viewing direction which is measured between the Line of Sight (LOS) and the nadir direction. For a sensor measuring in nadir ~~θ_L~~ θ_V is $0°$ and a sensor orientation close to the horizon is around ~~$\theta_L \approx 90°$~~ $\theta_V \approx 90°$. The relative solar azimuth angle ~~(RSAA)~~ ϕ represents the angle between LOS and the Sun direction. It is calculated from the difference of the azimuth angle of the Sun and the azimuth angle of the observation geometry of the optical inlets. For $\phi = 0°$ the LOS is pointing directly in the direction of the Sun and with $\phi = 180°$ the LOS is looking away from the sun.

For the RTS a typical mid-latitude cirrus with a cloud base height of 10 km and a cloud top height of 12 km is assumed. This closely represents the cloud situation which is investigated in Section 4. Calculations are performed for $\theta_0 = 25°, 50°$ and $75°$ representing three different scenarios. The relative solar azimuth angle is set to $\phi = 0°, 90°$ and $180°$.

The simulations are ~~performed~~ carried out with the radiative transfer package libRadtran 2.0 (Mayer and Kylling, 2005). The Fortran 77 discrete ordinate radiative transfer solver version 2.0 (FDISORT 2) after Stamnes et al. (2000) is ~~chosen~~selected to run the simulations. The incoming extraterrestrial solar flux density given by Gueymard (2004) is applied and molecular absorption is calculated using LOWTRAN (Pierluissi and Peng, 1985). ~~For the atmospheric aerosol concentration a~~ A marine aerosol profile is chosen (Shettle, 1989) and for vertical profiles of temperature, humidity, and pressure, a mid-latitude summer atmosphere profile is assumed. ~~For the simulations a spectral albedo~~ A spectral α typically for oceans is chosen according to

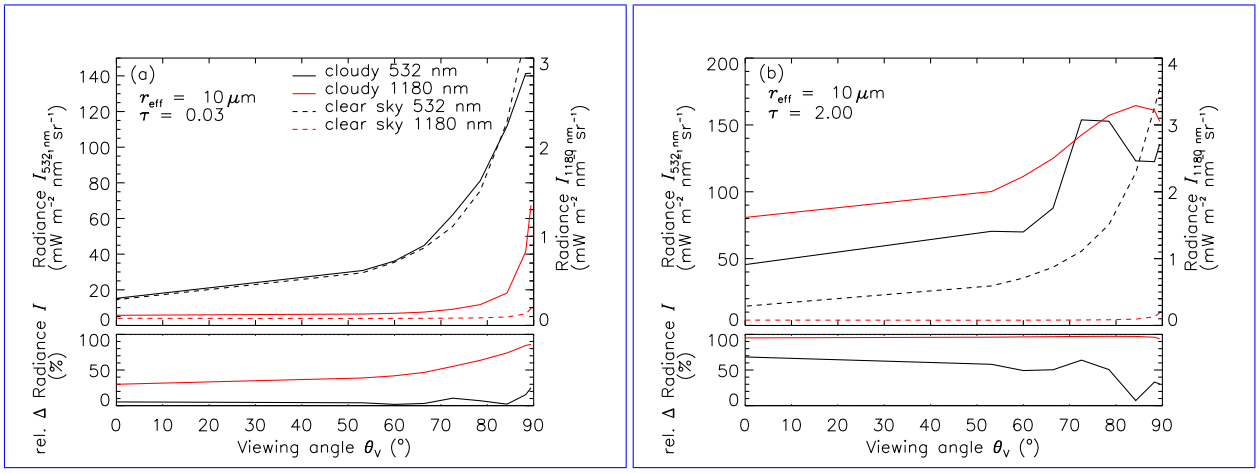

Figure 2. Simulated upward radiance ~~I_{RT}~~ I_{RTS} at λ = 532 nm and λ = 1180 nm for cloudy (solid line) and clear sky (dashed line) case as a function of the viewing angle ~~θ_L~~ θ_V. The left plot shows simulations for a SVC with $\tau = 0.03$ (a) and the right plot presents the simulations for a thick cirrus with $\tau = 2.0$ (b). In the corresponding lower ~~plot~~ plots the relative difference between cloud and clear sky atmosphere with respect to the cloudy atmosphere is shown.

~~the data of Clark et al. (2007). A~~ Clark et al. (2007). To represent ice crystals, a mixture of different particle shapes is used when not other specified. The ice crystal scattering phase function is parameterized according to Yang et al. (2013).

2.1 Wavelength sensitivity

~~For~~ Using solar spectral radiation for passive remote sensing ~~using solar radiation~~purposes, measurements at wavelengths sensitive to scattering and absorption by liquid water droplets and ice crystals are selected. Wavelengths less than λ = 900 nm are applied to retrieve τ from nadir ~~remote sensing. However, due to the increased photon path length of radiation reflected into any viewing angle off the nadir observation, absorption and scattering by atmospheric molecules becomes more pronounced. Figure 2~~radiance measurements. Figure 2a presents simulated upward ~~I_{RT}~~ radiances I_{RTS} reflected by an optically thin cirrus with $\tau = 0.03$ and ~~r_{eff} = 10 µm~~$r_{eff} = 10\ \mu$m, as well as clear sky radiance ~~for different sensor viewing angles. RTS~~ as a function of the sensor viewing angle. Radiative transfer simulations for two wavelengths, λ = 532 nm and λ = 1180 nm, are carried out. To easily distinguish the different geometries, simulated I in nadir geometry is denoted with ~~I^N_{RT}~~ I^N_{RTS}, while all geometries deviating from nadir are referred to ~~off-nadir~~ sideward viewing geometry and are indicated by ~~I^L_{RT}~~ I^V_{RTS}. The sensitivity ~~is measured by~~ ε_τ ~~defined as~~is defined by:

$$\varepsilon_\tau = \frac{\mathrm{d}I}{\mathrm{d}\tau} \tag{1}$$

~~For illustrating the impact of the cirrus on reflected I_{RT}, the difference of I_{RT} for the cloudy (solid line) and clear sky (dashed line) is shown.~~ In general, ~~I^L_{RT}~~ I^V_{RTS} increases with increasing ~~θ_L~~ θ_V due to the longer LOS. For a wavelength of $\lambda = 532$ nm,

no difference between cloudy and clear sky conditions is discernible for all ~~viewing angles~~θ_V, because Rayleigh scattering by molecules dominates and exceeds the scattering by thin cirrus. Therefore, at $\lambda = 532$ nm ~~cirrus~~ SVC with $\tau = 0.03$ which is presented in the simulations can not be detected. Conversely, for $\lambda = 1180$ nm ~~clear~~ separation between the simulations with and without cirrus at large viewing angles for ~~$\theta_L > 70°$~~ $\theta_V > 70°$ is present because the reflected ~~I^L_{RT}~~ I^V_{RTS} is increased due to larger LOS. At $\lambda = 1180$ nm wavelength Rayleigh scattering is comparable weak and does not significantly contribute to the reflected radiation. In nadir direction, a detection of ~~cirrus~~ SVC is not possible due to low τ, and the overwhelming backscattering from the ground.

For comparison, simulations of a thicker cirrus with $\tau = 2.0$ are presented in Figure 2b. Here, the influence of the Rayleigh scattering at $\lambda = 532$ nm is reduced and a distinction between cloudy and clear-sky conditions becomes possible. However, the relative difference between cloudy and clear-sky is still more pronounced at $\lambda = 1180$ nm.

The RTS suggest that ~~off-nadir observations for the detection of SVC and cirrus at near infrared~~ sideward viewing observations at near IR wavelengths ($\lambda > 900$ nm) are more suitable ~~.~~ for the detection of SVC and cirrus. As a result the retrieval in Section 4 is performed at 1180 nm and 1600 nm wavelength in the IR region which are sensitive to τ and r_{eff} and not disturbed by Rayleigh scattering.

2.2 Optical thickness and viewing angle

In general, back-scattered radiation by clouds increases with increasing τ. This sensitivity (see Eq. (1)) is the basis of most retrieval algorithms of cloud optical properties. To quantify how ε_τ is effected by ~~θ_L~~ θ_V of the sensor, RTS are performed for a set of different ~~θ_L ranging between $\theta_L = 0°$~~ θ_V ranging between $\theta_V = 0°$ (nadir) and ~~$\theta_L = 90°$ (off-nadir~~$\theta_V = 90°$ (sideward viewing). Cirrus optical thickness is varied in the range of τ = 0.03 - 4 covering various kinds of cirrus clouds.

~~Figure~~ First simulations presented in Fig. 3 displays simulated ~~$I_{RT,1180}$~~ $I_{RTS,1180}$ at $\lambda = 1180$ nm wavelength for two different $\theta_0 = 25°$ (a) and $\theta_0 = 75°$ (b) as a function of τ. For each scenario, ε_τ is calculated and given in the lower panels of Fig. 3. Simulations for nadir geometry are represented by solid black lines. Results for ~~off-nadir~~ sideward viewing sensor orientations are shown by dashed (~~$\theta_L = 53°$~~ $\theta_V = 53°$) and gray (~~$\theta_L = 78°$~~ $\theta_V = 78°$) lines. All scenarios show an increase of ~~I^L_{RT}~~ I^V_{RTS} for increasing τ, which results from enhanced reflection.

Due to the apparent longer LOS for both θ_0, ~~off-nadir~~ sideward viewing sensor orientations yield larger ε_τ of simulated ~~I^L_{RT}~~ I^V_{RTS} as compared to the nadir geometry ~~.~~ for cirrus clouds with $\tau \leq 1$ which includes SVC. This indicates that sideward measurements are most suited to retrieve τ below 1 and for the detection of SVC. The almost linear increase of the nadir radiance ~~I^N_{RT}~~ I^N_{RTS} indicates a constant ε_τ ~~in the range of investigated~~ for the investigated range of τ and θ_0~~presented here. In contrast, ε_τ for off-nadir simulations change with τ and~~ . For $\tau \geq 1$ the sensitivity of sideward viewing observations is in the same range compared to nadir measurements or slightly lower depending on the combination of θ_0 ~~as indicated by Fig. 3 (a) ($\theta_0 = 25°$) and Fig.3 (b) ($\theta_0 = 75°$).~~ and θ_V.

For low τ and a high sun, the highest ε_τ is given for the ~~off-nadir geometry ($\theta_L = 78°$)~~ sideward viewing geometry ($\theta_V = 78°$) for $\tau \leq 1$. A similar pattern emerges for low Sun ($\theta_0 = 75°$) resulting in larger ε_τ and a steep decrease for increasing τ. It shows that ε_τ decreases with τ and for ~~$\tau < 3$~~ $\tau \leq 2$ drops below ε_τ of nadir measurements~~for $\tau > 3$~~. The sensitivity of I with respect

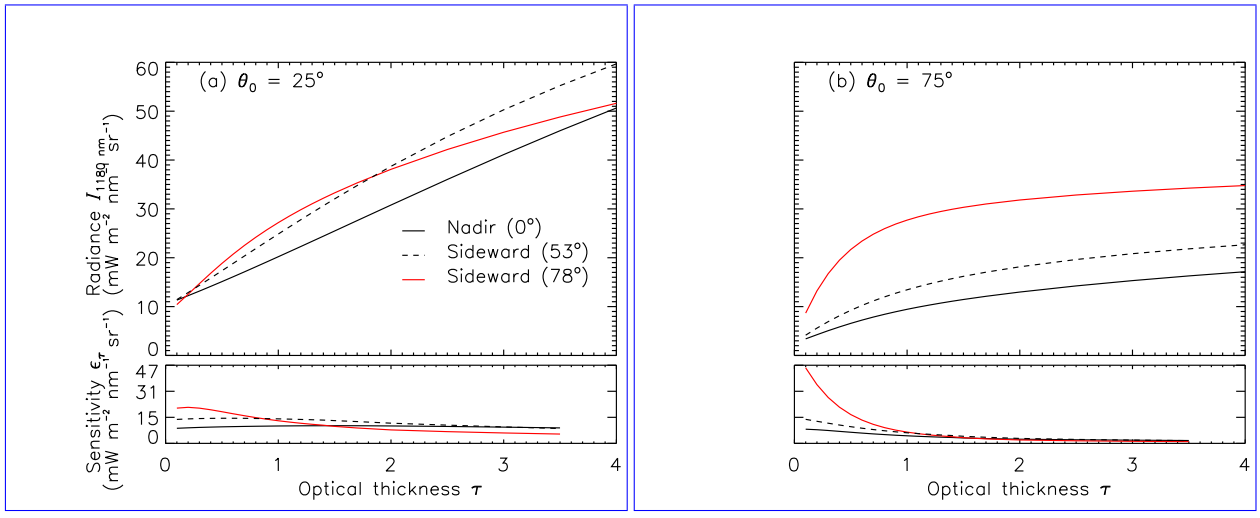

Figure 3. Simulated radiance $I_{\mathrm{RT},1180}$ for three different sensor orientations as a function of cirrus optical thickness τ. Results for solar zenith angles of $\theta_0 = 25°$ (a) and $\theta_0 = 75°$ (b) are displayed. The sensitivity ε_τ is given in the lower panels.

to τ can also be interpreted in terms of the uncertainty of retrieved τ related to an initial uncertainty in measured I. ~~A high~~ The higher ε_τ ~~leads to small retrieval uncertainties and vice versa.~~ the weaker the impact of uncertainties in the measurements on the uncertainties of the retrieved τ. As shown in Fig. 3b, a high ε_τ is calculated for $I_{\mathrm{RTS},1180}$ for $\tau \leq 1$ and indicates a lower measurement uncertainty. Therefore, sideward viewing observations at $\lambda = 1180$ nm allow a more accurate determination of τ compared to nadir observations for optical thin clouds with $\tau \leq 1$.

In a second step, the influence of ϕ is investigated on ~~$I^{\mathrm{L}}_{\mathrm{RT}}$~~ $I^{\mathrm{V}}_{\mathrm{RTS}}$ in respective simulations. Figure 4 shows ε_τ for a wide range of ~~θ_{L}~~ θ_{V} between 0° and 90° and ϕ between 0° and 180° for two clouds ~~of fixed cirrus optical thickness of~~ with $\tau = 0.1$ and $\tau = 2$ and two different SZA of $\theta_0 = 25°$ and $\theta_0 = 75°$. The ~~color code in Fig. 4 represents~~ graphs represent ε_τ in units of $\mathrm{mW\,m^{-2}\,nm^{-1}\,sr^{-1}}$ for different ϕ as a function of θ_{V}.

For $\tau = 0.1$ and $\theta_0 = 25°$ (Fig. 4~~(a)~~a, ε_τ ranges between 5 and 66 $\mathrm{mW\,m^{-2}\,nm^{-1}\,sr^{-1}}$. For ~~the optically thin cirrus ε_τ is insensitive to observation geometry for $\theta_{\mathrm{L}} < 60°$ and all ϕ. For larger θ_{L} (off-nadir~~ larger θ_{V} (sideward viewing observations) ε_τ increases significantly reaching the maximum for ~~$\theta_{\mathrm{L}} = 90°$~~ $\theta_{\mathrm{V}} = 90°$ and $\phi = 0°$. Observations under these angles are better suited in comparison to other angle combinations as they enable to achieve the largest possible ε_τ and reduced relative measurement errors which results in increased retrieval accuracy.

A similar pattern is derived for simulations assuming a lower Sun ($\theta_0 = 75°$) as shown in Fig. 4~~(b)~~b. Compared to $\theta_0 = 25°$ the increase of ε_τ for ~~$\theta_{\mathrm{L}} = 90°$~~ $\theta_{\mathrm{V}} = 90°$ and $\phi = 0°$ is stronger reaching values of 377 $\mathrm{mW\,m^{-2}\,nm^{-1}\,sr^{-1}}$ while for all other geometries ε_τ almost remains constant at the same magnitude reaching 80 $\mathrm{mW\,m^{-2}\,nm^{-1}\,sr^{-1}}$. Additionally, the maximum ε_τ is more concentrated on a single combination of ~~θ_{L}~~ θ_{V} and ϕ represented by the high peak for $\phi = 0$ compared to all other ϕ. Therefore, measurements in the range of these angles are recommended to achieve high values ε_τ for reasonable retrievals of τ.

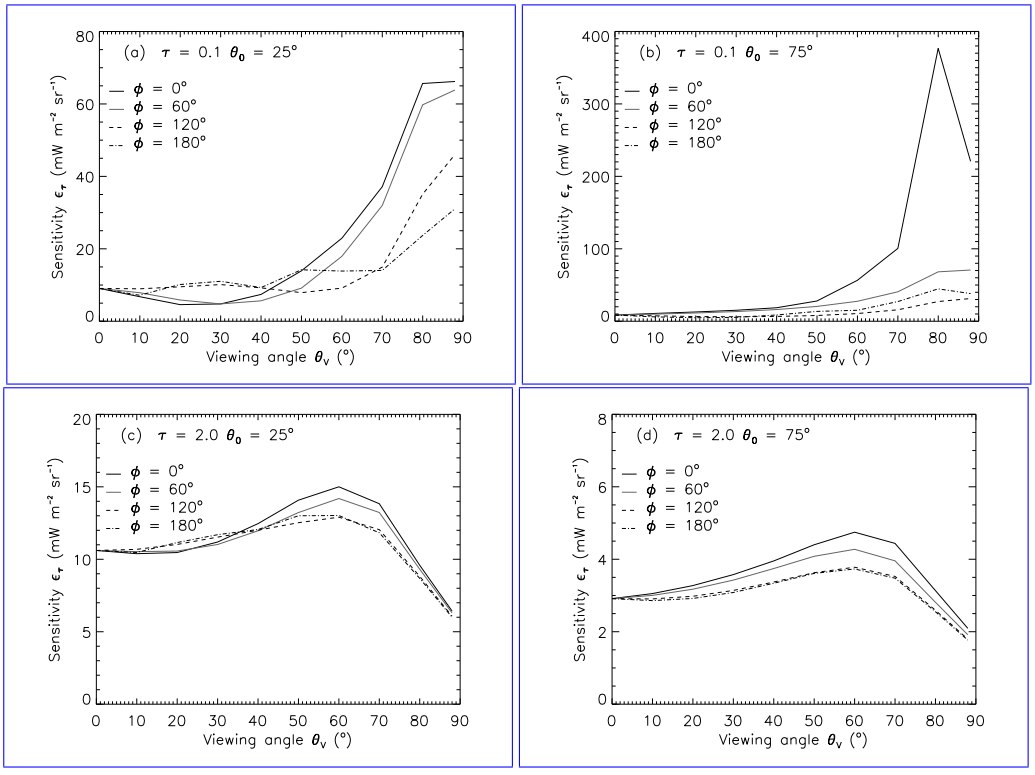

Figure 4. Sensitivity ε_τ at 1180 nm in units of $\mathrm{mW\,m^{-2}\,sr^{-1}}$ as a function of viewing angle ~~θ_L~~ θ_V and relative solar azimuth angle ϕ for cirrus optical thickness τ and solar zenith angle θ_0. Panel (a) for $\tau = 0.1$, $\theta_0 = 25°$, Panel (b) for $\tau = 0.1$, $\theta_0 = 75°$, Panel (c) for $\tau = 2$, $\theta_0 = 25°$ in (c) and Panel (d) for $\tau = 2$, $\theta_0 = 75°$. Different scales of the plots have to be considered.

Figure 4~~(c)~~ c shows the simulated ε_τ for clouds of $\tau = 2$, $\theta_0 = 25°$ and a wide range of geometries. Compared to the optically thin cirrus, ~~for optical thick cirrus~~ the maximum of ε_τ is reduced for optical thick cirrus not exceeding a value of 15 $\mathrm{mW\,m^{-2}\,nm^{-1}\,sr^{-1}}$ and shifted to smaller θ_0. While ~~off-nadir~~ sideward viewing measurements are predicted to become saturated for ~~thin~~ thick clouds, for ~~lower optical thickness the optimal viewing angle is about $\theta_L = 60°$~~ low τ the optimal θ_V is about $\theta_V = 60°$ with the largest ε_τ occurring for ϕ between 0° and 60°. Respective simulations for $\tau = 2$, $\theta_0 = 75°$ (low Sun) are presented in Fig. 4~~(d). Here~~d. Here, the maximum of ε_τ is small with 5 $\mathrm{mW\,m^{-2}\,nm^{-1}\,sr^{-1}}$ at θ_V and $\phi = 0$ compared to all other simulations varying τ and θ_0.~~Compared to simulations presented in Fig. 4 (c), the area with maximum ε_τ is concentrated between $\phi = 0°$ and $\phi = 30°$.~~

The RTS show that the choice of the best viewing geometry (nadir or ~~off-nadir~~ sideward viewing observations) strongly depends on τ and ϕ. In order to probe a large range of cirrus with sufficient large retrieval sensitivity, measurements in different viewing directions, at least in nadir and ~~off-nadir direction~~ sideward viewing direction depending on τ and θ_0 are recommended. ~~The strong angular dependence of off-nadir measurements for viewing angles $\theta_L = 90°$ requires~~ Measurements in sideward viewing geometry strongly dependent on θ_V especially around $\theta_V = 90°$. In order to avoid spurious results by mispointing

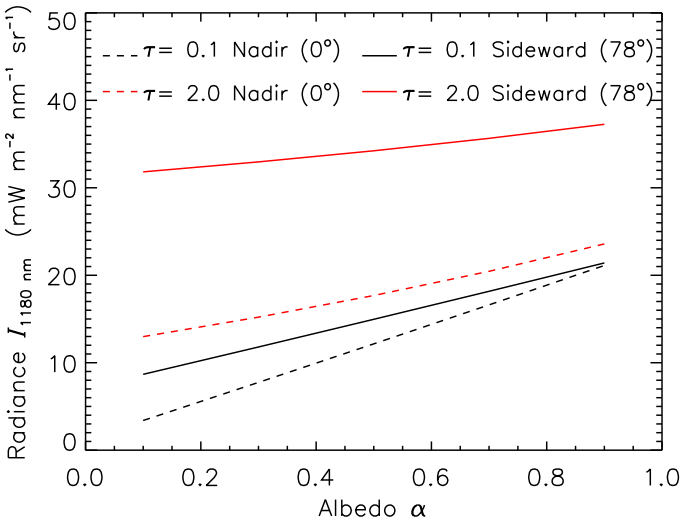

Figure 5. Influence of the surface albedo α on the measured upward radiance ~~$I^{\mathrm{L}}_{\mathrm{RT},1180}$~~ $I^{\mathrm{V}}_{\mathrm{RTS},1180}$ at λ = 1180 nm as a function of cirrus optical thickness τ and sensor orientation ~~θ_{L}~~ θ_{V}.

with the sensor, a careful alignment of the ~~telescope orientation in order to avoid spurious results~~optical sensor and an accurate determination is required. Considering these findings, the retrieval of τ in Section 4 is performed for $\theta_{\mathrm{V}} \leq 60°$ only.

2.3 Influence of surface albedo

The influence of α on the retrieval of cloud optical properties derived by passive remote sensing using the Moderate-resolution imaging spectroradiometer (MODIS) was investigated by Rolland and Liou (2001). They showed that ~~especially~~ retrievals of clouds with $\tau < 0.5$ are strongly influenced by variations in α. Based on RTS, Fricke et al. (2014) concluded that I^{N} measured in nadir direction strongly depends on the underlying surface reflectivity and that uncertainties in assumed α may cause errors of up to $50\,\%$ in the retrieval of τ.

In order to quantify and compare the influence of α on I measured in different ~~viewing angles~~ θ_{V} and nadir directions, RTS are performed. To cover the natural variability of surfaces ranging from ocean surface to ice-covered regions, α is varied between $\alpha = 0.1$ and $\alpha = 0.9$. ~~Fig.~~ Figure 5 shows simulated ~~$I^{\mathrm{L}}_{\mathrm{RT},1180}$~~ $I^{\mathrm{V}}_{\mathrm{RTS},1180}$ at λ = 1180 nm wavelength for two clouds with $\tau = 0.1$ and $\tau = 2$ and both observation geometries.

In general, the reflected I increases with increasing α. The stronger the increase, the stronger the measurements are effected by α. For both observation geometries, the steepest derivative,

$$\gamma = \frac{\mathrm{d}I}{\mathrm{d}\alpha}, \tag{2}$$

Table 1. Relative difference in ~~$I_{\mathrm{RT,1180\,nm}}$~~ $I_{\mathrm{RTS,1180\,nm}}$ for surface albedo $\alpha = 0.1$ and $\alpha = 0.9$ for different viewing angles ~~θ_{L}~~ θ_{V} and optical thickness τ.

	cirrus optical thickness		
viewing angle	$\tau = 0.1$	$\tau = 0.5$	$\tau = 2$
~~$\theta_{\mathrm{L}} = 0°$~~ $\theta_{\mathrm{V}} = 0°$	84 %	69 %	44 %
~~$\theta_{\mathrm{L}} = 78°$~~ $\theta_{\mathrm{V}} = 78°$	58 %	29 %	14 %

is obtained for the thin cirrus with $\tau = 0.1$. In general for increasing ~~optically~~ τ of thick clouds, α becomes less important for I compared to cirrus clouds with lower τ. To quantify the impact of changes in α, the relative difference between ~~I_{RT}~~ I_{RTS} simulated for $\alpha = 0.1$ and $\alpha = 0.9$ is calculated for each case and presented in Table 1. Maximum differences of up to 84 % are noticeable in nadir geometry for clouds of $\tau = 0.1$. Optically thick clouds show lower dependencies on α due to the increased contribution of radiation reflected by the cirrus. Comparing nadir and ~~off-nadir~~ sideward viewing geometries, the simulations show a smaller γ for ~~off-nadir observations~~ sideward viewing observations independent of α. The relative ~~differences of $I^{\mathrm{L}}_{\mathrm{RT}}$~~ difference of $I^{\mathrm{V}}_{\mathrm{RTS}}$ for $\tau = 2$ between $\alpha = 0.1$ and $\alpha = 0.9$ is reduced to 14 %. This indicates that I measured in ~~off-nadir~~ sideward viewing geometry is less influenced by changes in α (e.g., Oikarinen (2002)). This difference in I is most pronounced for optically thin clouds where the surface contribution to measured I is relatively large. Under unknown or variable surface albedo conditions, observations in ~~off-nadir~~ sideward viewing direction are favoured over those in nadir direction when retrieving the optical properties of thin cirrus.

2.4 Crystal shape sensitivity

By changing the ice crystal shape in the RTS (similar cloud as described above), the sensitivity of ~~radiance observation~~ I with respect to the ice crystal scattering phase function is investigated and compared for different viewing geometries. Ice crystals with shapes of columns, droxtals and plates are chosen and implemented in the simulations to cover the natural variability of cirrus based on the ice crystal single scattering properties provided by Yang et al. (2013). Most cirrus are composed of a mixture of ice crystal shapes (Pruppacher and Klett, 1997). Particle shape dependent scattering effects are lower due to smoothing over different crystal shapes. Therefore, an ice crystal mixture as given by Baum et al. (2005) is included in the simulations and serves as a reference. This is denoted with the acronym 'GHM' furtheron. The simulated ~~$I^{\mathrm{L}}_{\mathrm{RT,1180}}$~~ $I^{\mathrm{V}}_{\mathrm{RTS,1180}}$ as a function of ~~θ_{L}~~ θ_{V} is presented in ~~Fig. 6.~~ Fig. 6.

The increase of ~~$I^{\mathrm{L}}_{\mathrm{RT,1180}}$ with increasing θ_{L}~~ $I^{\mathrm{V}}_{\mathrm{RTS,1180}}$ with increasing θ_{V} is significantly influenced by the ice crystal shape. In the simulated cases, droxtals and the GHM ice crystal mixture show a larger increase of ~~$I^{\mathrm{L}}_{\mathrm{RT,1180}}$ with increasing θ_{L}~~ $I^{\mathrm{V}}_{\mathrm{RTS,1180}}$ with increasing θ_{V} than columns and plates. While in nadir geometry (~~$\theta_{\mathrm{L}} = 0°$~~ $\theta_{\mathrm{V}} = 0°$), columns and plates have a higher ~~$I^{\mathrm{L}}_{\mathrm{RT,1180}}$~~ $I^{\mathrm{V}}_{\mathrm{RTS,1180}}$ than droxtals and GHM, ~~$I^{\mathrm{L}}_{\mathrm{RT,1180}}$~~ $I^{\mathrm{V}}_{\mathrm{RTS,1180}}$ measured at viewing angles ~~$\theta_{\mathrm{L}} > 50°$~~ $\theta_{\mathrm{V}} > 50°$ is higher for droxtals and the GHM crystal mixture. The spatial distribution obtained for droxtals results from the enhanced forward and reduced sideways

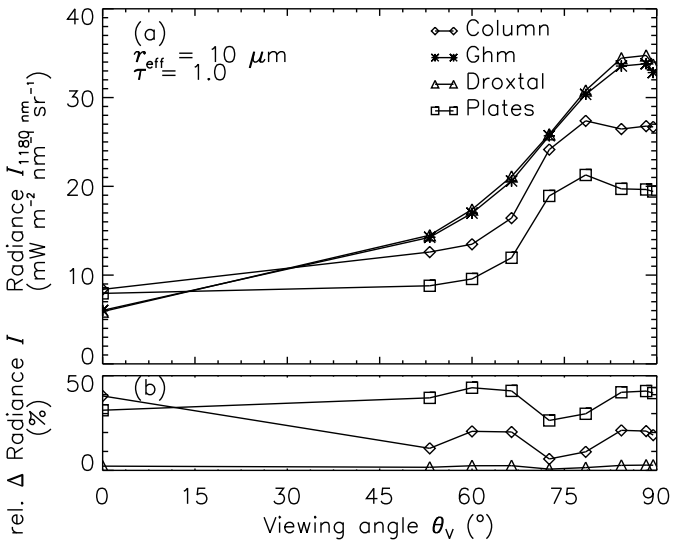

Figure 6. Simulated radiance ~~$I^{L}_{RT,1180}$~~ $I^{V}_{RTS,1180}$ at λ = 1180 nm wavelength for different ice crystal shapes as a function of the viewing angle ~~θ_L~~ θ_V of the sensor (a). In panel (b) the relative differences of simulated radiance with respect to the reference shape 'Ghm' is presented for the three other ice crystal shapes.

scattering compared to other crystal shapes.

For simulations in nadir direction the relative difference between lowest (droxtals) and highest (columns) ~~$I^{N}_{RT,1180}$~~ $I^{N}_{RTS,1180}$ differs by up to 41.5 % of the absolute radiance of ~~6.1 mW m^{-2} nm^{-1} sr^{-1}~~ 6.1 mW m^{-2} nm^{-1} sr^{-1} obtained by the 'GHM' crystal mixture.

For ~~off-nadir~~ sideward viewing observations the relative and absolute change in ~~$I^{L}_{RT,1180}$~~ $I^{V}_{RTS,1180}$ is even larger between ~~θ_L = 60° and θ_L = 90°~~ θ_V = 60° and θ_V = 90° . With increasing ~~θ_L~~ θ_V the differences of ~~$I^{L}_{RT,1180}$~~ $I^{V}_{RTS,1180}$ increase up to a maximum of 43.5 % at ~~θ_L = 78°~~ θ_V = 78° between droxtals and plates with respect to the absolute value of ~~33.8 mW m^{-2} nm^{-1} sr^{-1}~~ 33.8 mW m^{-2} for GHM.

The simulations show that the relative change in simulated ~~$I^{L}_{RT,1180}$~~ $I^{V}_{RTS,1180}$ due to ice crystal shape effects increases with ~~θ_L~~ θ_V. Therefore, for cirrus of low τ the interpretation of ~~off-nadir~~ sideward viewing observations rely even stronger on a correct assumption of ice crystal shape than nadir observations. Multiangular observations covering the angular pattern (Fig. 6), may provide sufficient information to retrieve ice crystal shape as proposed by Schäfer et al. (2013).

3 Airborne measurements

Simultaneous airborne measurements of I in nadir and ~~off-nadir~~ sideward viewing geometry were conducted during four campaigns using ~~the HALOresearch aircraft~~HALO. During NARVAL shallow convection in the North Atlantic trade-wind region

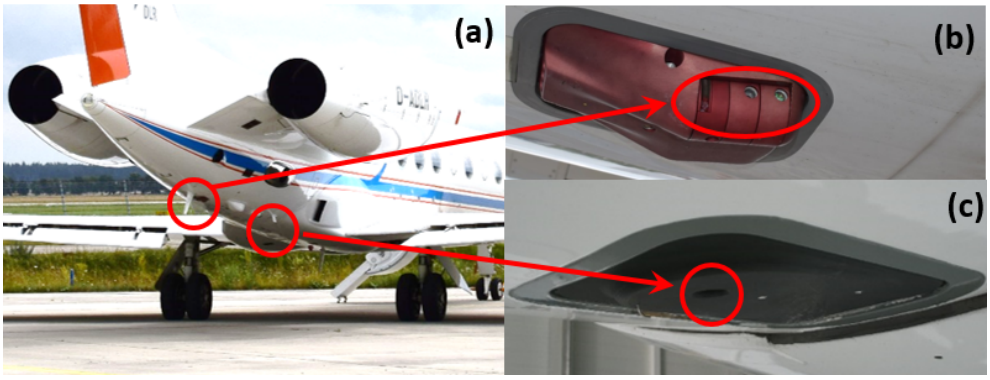

Figure 7. Optical inlets of mini-DOAS (b) and SMART (c) mounted at the lower aircraft fuselage.

of the northern Atlantic (NARVAL South, December 2013) and cloud systems associated with the North Atlantic mid-latitude stormtrack (NARVAL North, January 2014) were probed (Klepp et al., 2014). During the ML-CIRRUS campaign natural and contrail cirrus in the mid-latitudes ~~was~~ were investigated in March and April 2014 (Voigt et al., 2016). Deep convective clouds were observed during the Aerosol, Cloud, Precipitation, and Radiation Interactions and Dynamics of Convective Cloud Systems (ACRIDICON-CHHUVA) mission in September 2015 (Wendisch et al., 2016).

During these missions, a suite of different active and passive remote sensing instruments was operated on board HALO, including passive solar radiance measurements by SMART (Wendisch et al., 2016; Ehrlich et al., 2008) and the mini-DOAS (Hüneke et al., 2017). While SMART measured radiometrically calibrated radiance I_S^N in nadir direction, the mini-DOAS instrument simultaneously measures in nadir and varying sideward viewing directions in ~~ultra-violet (UV)~~UV/~~visible (VIS)~~VIS/~~near-infrared (IR)~~ IR wavelength ranges. The mini-DOAS measurements are traditionally analyzed by applying the ~~Differential optical absorption spectroscopy (DOAS)~~ DOAS technique. DOAS relies on an analysis of intensity ratios of two spectroscopic observations made under largely different atmospheric conditions. By exploiting ratios of I, DOAS measurements are inherently radiometrically calibrated in a relative but not absolute sense. Therefore no absolute radiometric calibration for I for the mini-DOAS is available. In addition to the two passive sensors, active lidar measurements with the Water Vapor Lidar Experiment in Space (WALES) were performed during NARVAL and ML-CIRRUS.

In Fig. 7~~(a)~~ a the position of the apertures at the aircraft fuselage is indicated. The optical inlets of mini-DOAS and SMART for upward radiation are shown in Fig. 7~~(b)~~ b and Fig. 7~~(c)~~ c respectively.

3.1 The SMART instrument

Depending on the configuration, SMART measures spectral upward ~~$F^{\uparrow}_{S,\lambda}$ S~~ $F^{\uparrow}_{S,\lambda}$ and downward irradiance $F^{\downarrow}_{S,\lambda}$, as well as spectral upward radiance I^N_S~~(Wendisch et al., 2001, 2016).~~ . The system is extensively described in Wendisch et al. (2001) and Ehrlich et al. (2008). In this paper the focus is on I^N_S measurements which are available for the four HALO missions introduced above.

Table 2. Individual sources of uncertainty and total uncertainties for the upward radiance $I^{N}_{S,1180}$ at a wavelength of λ = 1180 nm

.

	Source of Uncertainty	~~$\lambda = 1180$ nm~~ $\lambda = 1180$ nm
$I^{N}_{S,1180}$	Spectral Calibration	$< 1\,\%$
	Radiometric Calibration	$8.5\,\%$
	Signal-to-Noise-Ratio	$11.6\,\%$
	Transfer Calibration	$< 1.1\,\%$
	Total	$14.5\,\%$

To cover almost the entire solar spectral range, SMART measures I^{N}_{S} with two separate spectrometers, one for the ~~visible and near-infrared (VNIR)~~ VIS range from λ = 300 nm to λ = 1000 nm and a second one ~~sampling the shortwave infrared (SWIR)~~ for sampling the IR range from λ = 900 nm to λ = 2200 nm. ~~Merging~~ By merging the spectra, about $97\,\%$ of the solar spectrum is covered ~~(Bierwirth et al., 2009)~~(Bierwirth et al., 2009, 2010). The spectral resolution defined by the full width at half maximum (FWHM) is 8 - 10 nm for the ~~SWIR~~ IR spectrometer and 2 - 3 nm for the ~~VNIR~~ VIS spectrometer.

The radiance optical inlet of SMART has an opening angle of $\Delta = 2°$ and a sampling time of 0.5 s. Considering aircraft groundspeed and the distance of 500 m between the cloud and the aircraft the resulting footprint is about 18 x 110 m for an individual I^{N}_{S} measurement. For a distance of 1000 m between sensor and cloud the footprint increases to 35 x 220 m.

Prior to each campaign SMART was radiometrically calibrated in the laboratory using certified calibration standards traceable to NIST and by secondary calibration using a travelling standard during the operation on HALO. The total measurement uncertainty of I^{N}_{S} is about $5.4\,\%$ for the ~~VNIR~~ VIS and $14.5\,\%$ for the ~~SWIR~~ IR range which consist of individual errors due to the spectral calibration, the spectrometer noise and dark current, the radiometric calibration and the transfer calibration (Brückner et al., 2014). In Table 2 the contributions of each individual source of uncertainty is given for measurements at λ = 1180 nm wavelength. The main uncertainty results from the Signal-to-Noise-Ratio (SNR) and the calibration standard, while spectral and transfer calibration errors are almost negligible. Averaging a time series of measurements will reduce the contribution of sensor noise to the signal.

3.2 The mini-DOAS instrument

The mini-DOAS is a passive airborne remote sensing system originally designed to retrieve vertical profiles of trace gases, aerosol and cloud particles (Hüneke et al., 2017). The analyzis is based on the ~~Differential Optical Absorption Spectroscopy (DOAS)~~ DOAS technique that applies least square retrievals on the spectral shape of the observed ~~I^{L}_{mD}~~ upward radiance I^{V}_{mD} by the mini-DOAS in sideward viewing channels (Platt and Stutz, 2008). Spectral absorption bands of molecules and particles are measured at moderate spectral resolution (FWHM ~~0.1 nm~~= 0.47 nm, 1.2 nm, 10 nm for the UV, VIS and IR, respectively) to quantify the absorption of solar radiation by trace gases along the light path. DOAS measurements are primarily used to ~~estimate~~ infer trace gas concentrations and associated photochemistry in the atmosphere. Here, measured ~~I^{L}_{mD}~~ I^{V}_{mD} are employed

for the remote sensing of clouds.

The mini-DOAS is designed as a compact, lightweight and robust system to be operated aboard ~~the HALOaircraft~~HALO. The instrument consists of six telescopes which are connected via fiber bundles to six optical spectrometers. One set of the optical inlets is fixed in nadir configuration while the other telescopes can be tilted between ~~$\theta_L = 0°$ and $\theta_L = 90°$~~$\theta_V = 0°$ and $\theta_V = 90°$. Two sets of three different spectrometers are applied to cover the ~~ultraviolet (UV)~~ UV spectral range from 310 nm to 440 nm (FWHM 0.5 nm), the ~~visible (VIS)~~ VIS range from 420 nm to 650 nm (FWHM 1 nm) and the ~~near infrared (SWIR)~~ IR range from 1100 nm to 1680 nm (FWHM ~~5~~ 10 nm). In the UV and VIS range Charged-Coupled Devices (CCD) sensors are used as detectors. The detection in the ~~SWIR~~ IR range is performed by Photo Diode Arrays (PDA).

The telescopes are mounted on an aperture plate at the lower side of the aircraft fuselage. The scanning telescopes have rectangular fields of view of about $0.6°$ in vertical direction and $3°$ in horizontal direction. During scanning measurements the telescopes are directed to the starboard side of the aircraft. Changes of aircraft roll angles are compensated within ~~0.1°~~0.2°. The orientation of the nadir telescope is kept fix with respect to the aircraft major axis. Therefore no compensation of the aircraft roll angle is performed.

The evacuated spectrometer housing is immersed into an isolated water / ice tank to ensure a constant temperature and pressure of the spectrometers independent from changing outside conditions. Evacuation of the housing and temperature stabilization is necessary to guarantee a stable optical imaging, which is indispensable for DOAS applications. A spectral calibration of the spectrometers assures that wavelength shifts are less than 0.05 nm.

3.3 The WALES instrument

The Water Vapor Lidar Experiment in Space Demonstrator (WALES) is an airborne Differential Absorption Lidar (DIAL) with additional aerosol and cloud detection capabilities operated on the German research aircraft Falcon and HALO (Wirth et al., 2009).

For particle detection WALES has two backscatter and depolarization channels at λ = 532 nm and λ = 1064 nm wavelength and an additional high spectral resolution lidar (HSRL) channel at λ = 532 nm (Esselborn et al., 2008). The HSRL channel allows the retrieval of the backscatter coefficient of clouds at λ = 532 nm without assumptions about the phase function of the cloud particles. ~~Also the apparent transmission of the cloud can easily be determined from the HSRL-channel. If multiple scattering effects are neglected this apparent transmission is simply the exponential of the negative optical thickness.~~ Unfortunately, larger cirrus particles usually show a pronounced forward scattering peak, which may contain a significant fraction of the scattered energy. This may lead to an underestimation of τ calculated from the individual particle extinction cross sections (see e.g. (Platt, 1981)). The optical thickness data presented in this paper are corrected for the forward scattering effect following the algorithm proposed by Eloranta (1998). To apply this correction scheme, an ~~effective particle radius~~ r_{eff} is assumed, which determines the width of the forward scattering peak. Best compensation of the multiple scattering decay below the cloud ~~was~~ is found for $r_{\text{eff}} = 35 \pm 5\,\mu\text{m}$ in good agreement with the climatological values proposed by Bozzo et al. (2008). The mean correction factor for the data set shown in this paper was $7\,\%$.

4 Cross-calibration

Since no radiometric calibration is available for mini-DOAS, simultaneous measurements of SMART and mini-DOAS are used to cross-calibrate ~~both instruments~~the mini-DOAS with SMART. The cross-calibration relies on the radiometric calibration of SMART and allows to derive calibrated I_{mD} from mini-DOAS measurements. Flight sections with inhomogeneous α and various cloud conditions are selected to obtain a calibration valid for a wide range of different I. Such conditions were present during the ML-CIRRUS flight on the 26 March 2014 including measurements over southern Germany, Belgium, United Kingdom, Ireland and the northern Atlantic Ocean westerly of Ireland. The cross-calibration is performed for ~~nadir and off-nadir viewing geometries of~~ the nadir and sideward viewing scanning telescopes of the mini-DOAS when aligned to the same cloud area as SMART. The results are presented for two wavelengths at λ = 1180 nm and λ = 1600 nm which are frequently used in cloud retrievals and show best discrimination potential for small τ as presented in the sensitivity study. Different FWHM of both spectrometer systems are considered by convoluting the spectrally higher resolved measurements of the mini-DOAS with the corresponding FWHM of the SMART spectrometer (8-19 nm).

4.1 Nadir radiance

The nadir sensors of the mini-DOAS operate in fixed position, thus providing a large data set of simultaneous measurements with SMART. The time stamps of both instruments are corrected for temporal offsets in the data acquisition. Scatter plots of $I^{\mathrm{N}}_{\mathrm{S},\lambda}$ and mini-DOAS raw data are shown in Fig. 8a and Fig. 8c for both wavelengths. For each data point a linear regression after Theil (1992) and Sen (1968) is performed. Using the method after Theil and Sen the influence of outliers on the regression is reduced and the linear calibration equation $I^{\mathrm{N}}_{\mathrm{S},\lambda} = a_0 \cdot N^{\mathrm{N}}_{\mathrm{mD},\lambda} + a_1$ for the mini-DOAS radiances are determined. $I^{\mathrm{N}}_{\mathrm{S},\lambda}$ is the radiance measured by SMART, $N^{\mathrm{N}}_{\mathrm{mD},\lambda}$ the raw signal of mini-DOAS and a_0 and a_1 the calibration coefficients. The linear regressions are indicated by the gray lines in Fig. 8~~(a)~~ a and Fig. 8~~(c)~~c. For the ML-CIRRUS flight on 26 March 2014 the nadir geometry calibration coefficients are determined as ~~$a_0 = 0.31\,\mathrm{mW\,m^{-2}\,sr^{-1}}$ and $a_1 = 0.55\,\mathrm{mW\,m^{-2}\,sr^{-1}}$~~ $a_0 = 0.31\,\mathrm{mW\,m^{-2}\,sr^{-1}}$ and $a_1 = 0.55\,\mathrm{mW\,m^{-2}\,sr^{-1}}$ for λ = 1180 nm with an uncertainty of ~~$\pm 0.24\,\mathrm{mW\,m^{-2}\,sr^{-1}}$~~ $\pm 0.24\,\mathrm{mW\,m^{-2}\,sr^{-1}}$. Similar calibrations are performed for flights during the NARVAL and ACRIDICON-CHUVA campaigns. All calibration coefficients are summarized in Table 3. The coefficients depend on various environmental condition where the temperature dependence of the mini-DOAS spectrometers is the most influencing parameter.

The uncertainty is mostly related to differences of the FOV and the related difference in the observed scene and possible minor mismatches of the nadir orientation of both sensors. This means that both sensors do not always observe the exact same cloud area. For the λ = 1600 nm wavelength, a_0 is higher compared to λ = 1180 nm in all analyzed flights indicating the different spectral sensitivities of both sensors with SMART in comparison with mini-DOAS ~~beeing~~ being relatively more sensitive at λ = 1600 nm than at λ = 1180 nm wavelength.

The derived cross-calibrations of mini-DOAS are applied to all mini-DOAS measurements. A measurement example of a time series of calibrated mini-DOAS radiances ~~I_{mD}~~ $I^{\mathrm{N}}_{\mathrm{mD},\lambda}$ is shown in Fig. 8~~(b) and 8(d)~~ b and 8d for a 18 minute flight section measured on the 26 March 2014.

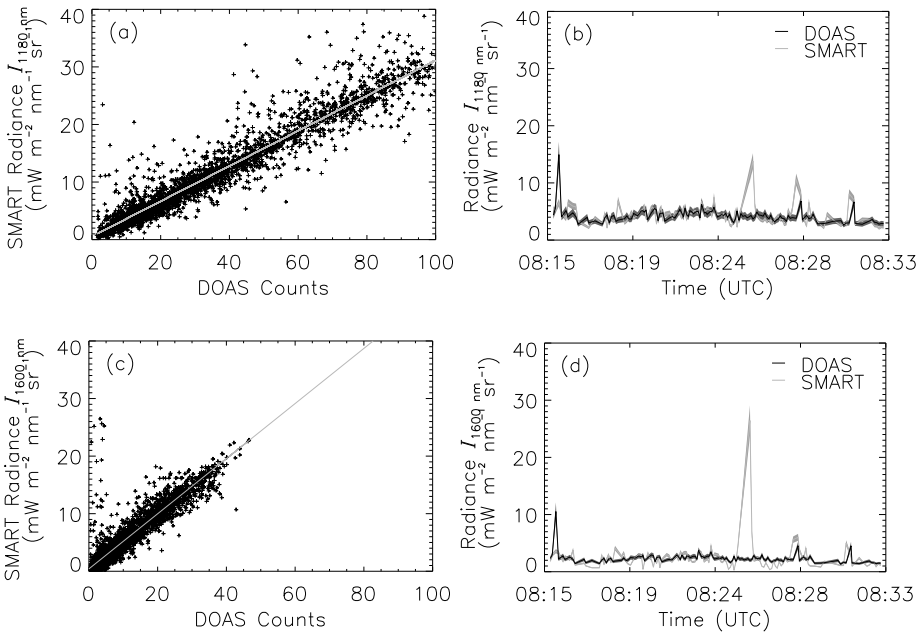

Figure 8. Panel (a) and (c) show comparisons of SMART radiance I_S^N and mini-DOAS raw signal for nadir channels at $\lambda = 1180$ nm and $\lambda = 1600$ nm wavelength. Panel (b) and (d) show time series of measured SMART radiance $I_{S,\lambda}^N$ and calibrated mini-DOAS radiance ~~$I_{mD,\lambda}^L$~~ $I_{mD,\lambda}^N$ for the ML-CIRRUS flight on 26 March 2014. The shaded areas indicate the measurement uncertainties.

The radiance time series for $\lambda = 1180$ nm of both sensors agree within the SMART error range for most data points, except for some radiance peaks. These differences likely result from the different FOV of both instruments and the presence of patches of low cumulus with high reflectivity. A similar result is obtained for $\lambda = 1600$ nm. The differences of the mean radiance between both instruments for the time period presented in Fig. 8 is ~~$0.75\,\mathrm{mW\,m^{-2}\,nm^{-1}\,sr^{-1}}$~~ $0.75\,\mathrm{mW\,m^{-2}\,nm^{-1}\,sr^{-1}}$ at $\lambda = 1180$ nm and ~~$0.5\,\mathrm{mW\,m^{-2}\,nm^{-1}\,sr^{-1}}$~~ $0.5\,\mathrm{mW\,m^{-2}\,nm^{-1}\,sr^{-1}}$ at $\lambda = 1600$ nm ~~.~~ which results in relative differences of 5.4 % at $\lambda = 1180$ nm and 1.9 % at $\lambda = 1600$ nm compared to the SMART absolute values.

4.2 ~~Off-nadir~~ Sideward viewing radiance

The scanning telescopes of the mini-DOAS typically run in a sequential mode scanning different ~~θ_L~~ θ_V. During selected flight segments the scanning sequences are configured to include nadir measurements. Due to this sequential mode less measurements from the ~~off-nadir~~ sideward viewing channels are available for cross-calibration with SMART because only measurements in nadir sensor orientation are applicable for the cross-calibration. To ensure a statistically sufficient number of samples, the entire flight of 26 March 2014 is analyzed applying the same methods used for the calibration of the nadir channels. ~~Figures 9 (a) and 9 (c)~~ Figures 9a and 9c show the cross-calibration of SMART radiances $I_{S,\lambda}^N$ and mini-DOAS raw data ~~$N_{mD,\lambda}^L$~~ $N_{mD,\lambda}^V$ and the linear fit (gray line) used for calibration. For the ~~s near infrared~~ IR scanning channels the calibration coefficients

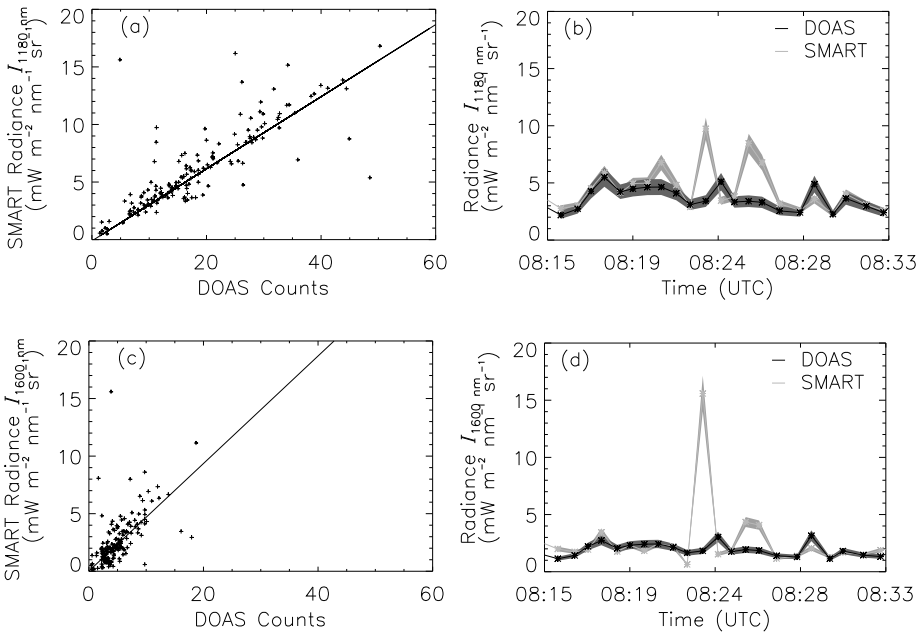

Figure 9. Panel (a) and (c) show a comparison of SMART radiance $I^{N}_{S,\lambda}$ and mini-DOAS raw signal ~~$N^{L}_{mD,\lambda}$~~ $N^{V}_{mD,\lambda}$ for the scanning channels at λ = 1180 nm and λ = 1600 nm wavelength. Panel (b) and (d) show time series of measured SMART radiance $I^{N}_{S,\lambda}$ and calibrated mini-DOAS radiance ~~$I^{L}_{mD,\lambda}$~~ $I^{V}_{mD,\lambda}$ for the ML-CIRRUS flight on 26 March 2014. The shaded areas indicate the measurement errors.

are determined as ~~$a_0 = 0.31\,\mathrm{mW\,m^{-2}\,sr^{-1}}$~~ $a_0 = 0.31\,\mathrm{mW\,m^{-2}\,sr^{-1}}$ with no offset a_1 for λ = 1180 nm and an uncertainty of ~~$\pm 0.2\,\mathrm{mW\,m^{-2}\,sr^{-1}}$~~ $\pm 0.2\,\mathrm{mW\,m^{-2}\,sr^{-1}}$. Similar to the nadir channels, the calibration coefficients for the the ~~off-nadir~~ sideward viewing channel at λ = 1600 nm wavelength with $a_0 = 0.47$ are higher compared to the λ = 1180 nm wavelength.

The calibration of the ~~off-nadir~~ sideward viewing channels is repeated for the NARVAL flights while for all ACRIDICON-CHUVA flights no nadir observations of the ~~off-nadir~~ sideward viewing channels are available. Table 3 provides a summary of all calibration coefficients derived for the ~~off-nadir~~ sideward viewing channels.

Similar to Fig. 8b and Fig. 8d, Figures 9~~(b) and 9(d)~~ b and 9d show time series of SMART radiance $I^{N}_{S,\lambda}$ and calibrated mini-DOAS nadir observations ~~$I^{N}_{mD,\lambda}$~~ of $I^{V}_{mD,\lambda}$ with the sideward viewing channels for a 18 minutes flight segment of the ML-Cirrus on 26 March 2014. In general, the radiance pattern observed by SMART is represented by the calibrated mini-DOAS radiance. However, individual data points differ due to differences in FOV resulting in mean differences of ~~$0.78\,\mathrm{mW\,m^{-2}\,nm^{-1}\,sr^{-1}}$~~ $0.78\,\mathrm{mW\,m^{-2}\,nm^{-1}\,sr^{-1}}$ at 1180 nm and ~~$0.38\,\mathrm{mW\,m^{-2}\,nm^{-1}\,sr^{-1}}$~~ $0.38\,\mathrm{mW\,m^{-2}\,nm^{-1}\,sr^{-1}}$ at λ = 1600 nm which results in relative differences of 3.7% at λ = 1180 nm and 2.4% at λ = 1600 nm compared to the SMART absolute values. This ranges below the uncertainty range of SMART.

Table 3. Calibration coefficients a_0 and a_1 in units of $\mathrm{mW\,m^{-2}\,nm^{-1}\,sr^{-1}}$ for mini-DOAS nadir and scanning channel radiance obtained for NARVAL (19 December 2013), ML-CIRRUS (26 March 2014) and ACRIDICON-CHUVA (9, 12 and 23 September 2014).

	1180 nm				1600 nm			
	Nadir		sideward viewing		Nadir		sideward viewing	
	$(\mathrm{mW\,m^{-2}\,nm^{-1}\,sr^{-1}})$							
	a_0	a_1	a_0	a_1	a_0	a_1	a_0	a_1
NARVAL (19.12.)	0.26	5.40	0.23	0.90	0.28	1.32	0.26	0.10
ML-CIRRUS (26.03.)	0.31	0.55	0.31	0.00	0.43	0.25	0.47	0.02
ACRIDICON-CHUVA (09.09)	0.24	5.28			0.37	2.80		
ACRIDICON-CHUVA (12.09.)	0.34	0.94			0.51	0.77		
ACRIDICON-CHUVA (23.09.)	0.31	3.43			0.40	0.59		

4.3 Temporal stability of cross-calibration

The mini-DOAS instrument is not explicitly designed to maintain a stable radiometric calibration but ~~this~~ more for a stable wavelength calibration. For DOAS measurements absolute values of I are not needed as only relative intensities are used. More important is the wavelength accuracy to determine absorption and emission bands of gasses precisely. As a result the radiometric calibration of the mini-DOAS can change from campaign to campaign and even between several flights. Therefore, cross-calibration coefficients for different campaigns and flights are derived to consider ~~changes of~~ these changes of radiometric calibration and the optical setup, for example when changing the optical fibers. Using different calibration factors for the mini-DOAS instrument as inferred for the different campaigns, Fig. 10 shows a comparison of measured I at λ = 1180 nm wavelength from a four minutes long flight segment over the Amazon region on 12 September 2014. The comparison clearly indicates that the measurements of I of both sensors are not systematically biased and agree within the errors of each sensor except when differences at small spatial scales appear resulting from the different FOV.

The deviation of the different calibrations is below ~~$2.9\,\mathrm{mW\,m^{-2}\,nm^{-1}\,sr^{-1}}$ indicating~~ $2.9\,\mathrm{mW\,m^{-2}\,nm^{-1}\,sr^{-1}}$ which is inside the measurement uncertainties of SMART and indicates a reasonable stability of the calibrations. ~~This suggests, that the calibration coefficients do not change significantly with time and the mini-DOAS calibration is relatively constant.~~

5 Retrieval of cirrus optical thickness

5.1 Iterative algorithm

By using all three calibrated radiance data sets obtained from SMART $I^{\mathrm{N}}_{\mathrm{S}}$, mini-DOAS nadir channels $I^{\mathrm{N}}_{\mathrm{mD}}$, and ~~off-nadir channels $I^{\mathrm{L}}_{\mathrm{mD}}$~~ sideward viewing channels $I^{\mathrm{V}}_{\mathrm{mD}}$, an iterative retrieval algorithm of τ is developed and applied. It is based on the bi-spectral reflectance method described by Twomey and Seton (1980), and Nakajima and King (1990). Here~~it was~~, the

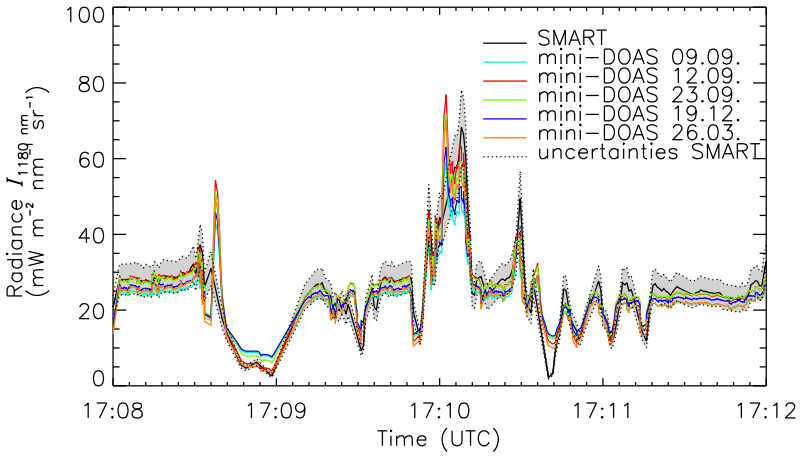

Figure 10. Time series of the nadir radiance of SMART $I^{\mathrm{N}}_{\mathrm{S},1180}$ and of the mini-DOAS $I^{\mathrm{N}}_{\mathrm{mD},1180}$ nadir channel at λ = 1180 nm using different calibrations as indicated in the legend. The uncertainty range of SMART radiance is shaded gray.

retrieval is adapted for ice clouds with respect to ice crystal shape and used ~~wavelength~~wavelengths, e.g. by Ou et al. (1995) and Rolland et al. (2000). For retrieving τ rough aggregates are assumed using pre-calculated ice crystal parametrizations after Yang et al. (2013). The iterative algorithm utilizes the spectral reflectivity $\mathcal{R}_\lambda$ which is defined as the ratio of spectral upward I_λ to spectral downward $F^{\downarrow}_\lambda$,

$$\mathcal{R}_\lambda = \frac{I_\lambda \pi}{F^{\downarrow}_\lambda} \tag{3}$$

~~During~~ For the ML-CIRRUS data, $F^{\downarrow}_\lambda$ is taken from the actual SMART measurements on HALO. Measured $F^{\downarrow}_\lambda$ allows to identify and eliminate any influence of the radiation field above the aircraft, for example by cirrus. As an alternative to pre-calculate Look-up-Tables (LUT) by extensive forward simulations, an iterative algorithm is applied that runs RTS adjusted to each single measurement. This allows to set up simulations by actual input parameters for each measurement ~~i.~~ e.g. θ_0, ϕ, longitude, latitude and flight altitude. In that way, uncertainties caused by inaccurate assumptions in the RTS input are minimized. Additionally, the iterative method is not limited to a specific pre-calculated grid of τ and r_{eff} as used in LUTs where a certain interval of preselected τ and r_{eff} are given. The iterative algorithm automatically adjusts the range of τ and r_{eff} without interpolation until reaching the final result.

Figure 11 shows a scheme of the retrieval algorithm, which starts with an initial guess of τ_0. Using the initial guess of τ and of any other cloud parameters, the cloud reflectivity $\mathcal{R}_{\mathrm{sim}}$ is simulated and compared to the measurements $\mathcal{R}_{\mathrm{meas}}$ of SMART and mini-DOAS, respectively. The ratio between $\mathcal{R}_{\mathrm{sim,n}}$ and $\mathcal{R}_{\mathrm{meas}}$ derived for each iteration step n is used to scale the particular

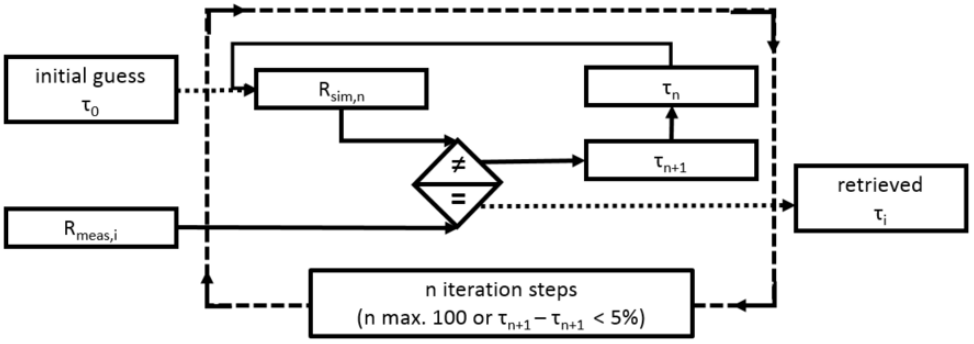

Figure 11. Scheme of the iterative algorithm. For every single measurement i an iteration loop is started with an initial guess τ_0 until measured $\mathcal{R}_{\text{meas}}$ and simulated $\mathcal{R}_{\text{sim}}$ reflectivity converge within $5\,\%$ difference or a maximum of 100 iteration steps is reached. At the end of the process the result is saved.

guess τ_n by

$$\tau_{n+1} = \tau_n \cdot \frac{\mathcal{R}_{\text{sim}}}{\mathcal{R}_{\text{meas}}}. \tag{4}$$

The adjusted ~~optical thickness~~ τ_{n+1} is used in the RTS for the new iteration step $n+1$. The iteration of τ is repeated until the change of τ_n between two iteration steps is smaller than $5\,\%$ or a limit of $n > 100$ iteration steps is reached. These stop criteria determine the accuracy of the iterative retrieval. If a lower relative stop criteria (change of τ_n smaller than $5\,\%$ between two iteration steps or more then 100 iteration steps) is used the iteration may come closer to the true searched value and the retrieval accuracy increases as well as the necessary iteration steps and the computational time. To limit the computational time, the second stop criteria is used to limit the maximum number of iteration steps. For a typical cirrus observed during ML-CIRRUS with an average τ of 0.32, the cirrus optical thickness can be retrieved with a accuracy of about $\tau \pm 0.03$. The retrieval of τ by SMART and mini-DOAS bases on the measurements at $\lambda = 1180$nm and is scaled to $\lambda = 532$ nm to consider the wavelength dependence of τ and to be able to compare it with WALES measurement at $\lambda = 532$ nm. Therefore, the retrieval considers RTS at both wavelengths. In the RTS τ is defined and changed at $\lambda = 532$ nm while the measurements are compared to simulations at $\lambda = 1180$ nm to determine the correct solution.

In case of measurements of optically thin cirrus, the retrieval can be applied for τ only. For these situations ~~the nadir radiance~~ $I^{\text{N}}_{\text{RTS,1600}}$ at λ = 1600 nm wavelength (ice absorption band) ~~to retrieve r_{eff} is~~ is too low and only measured with high uncertainty to retrieve r_{eff}. For a cirrus cloud with $\tau = 0.03$, ~~$I^{\text{N}}_{\text{RT,1600}}$~~ the simulated upward ~~I is~~ nadir radiance $I^{\text{N}}_{\text{RTS,1600}}$ and the sideward viewing radiance $I^{\text{V}}_{\text{RTS,1600}}$ in the range of ~~$0.2\,\text{mW}\text{m}^{-2}\text{sr}^{-1}$~~ $0.2\,\text{mW}\text{m}^{-2}\text{sr}^{-1}$. Such low I are in the range of the electronic noise of the spectrometers leading to low Signal-to-Noise-Ratio and high retrieval uncertainties. Especially for cirrus with low τ the variation of ~~$I^{\text{N}}_{\text{RT,1600}}$~~ $I^{\text{N}}_{\text{RTS,1600}}$ and $I^{\text{V}}_{\text{RTS,1600}}$ with respect to changes in r_{eff} is low.

Simulations show, that for $\tau = 0.5$ the difference of ~~$I^{\text{N}}_{\text{RT,1600}}$~~ $I^{\text{N}}_{\text{RTS,1600}}$ in nadir direction is only ~~$0.1\,\text{mW}$~~ $0.1\,\text{mW}$ when changing r_{eff} from ~~$10\,\mu\text{m}$ to $20\,\mu\text{m}$~~ $10\,\mu\text{m}$ to $20\,\mu\text{m}$ indicating the low sensitivity of r_{eff} retrievals at this wavelength. Therefore,

a reliable retrieval of r_{eff} with reasonable accuracy is not feasible. ~~In the retrieval algorithm~~ For $I^{\text{V}}_{\text{RTS},1600}$ the difference is $1.4\,\text{mWm}^{-2}\text{sr}^{-1}$ and about a magnitude larger indicating that a retrieval of r_{eff} ~~is fixed to $30\,\mu$m~~ might be reasonable. However, in order to be consistent between both nadir and sideward viewing retrieval, r_{eff} has been fixed. A value of $r_{\text{eff}} = 30\,\mu$m was chosen, a typical value of ice crystals observed by in-situ measurements during ML-CIRRUS (Voigt et al., 2016). Therefore, the influence of an invalid assumption of r_{eff} on the iterative retrieval is analyzed. For this purpose the retrieval is tested for a typical cirrus of $\tau = 0.3$ ~~.~~and is run with three different assumptions of r_{eff} of ~~$20\,\mu$m, $30\,\mu$m, $40\,\mu$m~~$20\,\mu$m, $30\,\mu$m, $40\,\mu$m, representing the uncertainty of r_{eff}. These simulations imply that the retrieved τ changes only by ± 0.02 between smallest and largest r_{eff}, resulting in a relative error in τ of $6.7\,\%$. The uncertainty in measured $I^{\text{N}}_{\text{S},1600}$ and $I^{\text{V}}_{\text{mD},1600}$ causes a retrieval uncertainty of ~~$\tau \pm 0.02$~~less than $\tau \pm 0.2$. This justifies the fixed choice of r_{eff} in this specific cloud case.

However, the dependence of retrieved τ and the assumption of r_{eff} may vary with α, ice crystal size, τ and λ used in the retrieval.

5.2 ML-CIRRUS case study

The iterative retrieval is applied for a selected leg of the ML-CIRRUS flight on 26 March 2014. For this day the Terra MODIS image (overpass time 10:40 UTC) indicates ~~the cloud~~clouds, with a west to east gradient in τ ranging from 5.8 to 0.38 (Fig. 12) ~~. In the figure the~~ including small cloud free regions. For large areas, cirrus with $\tau \leq 1$ is indicated by MODIS providing provides a well suited test case to compare sideward viewing and nadir observations even when τ ranges above the SVC level. As discussed in Section 2, for low τ ranging up to 1, ε_τ of sideward viewing observations is higher than for nadir observations. An advantage of using a test case with τ higher than SVC is the insensitivity of the retrieval uncertainty with respect to the radiance measurement uncertainty. The reflected I is still sufficiently large and exceeds the noise level of the nadir looking instruments to make a comparison between nadir and sideward viewing instruments possible.

In Figure 12 the flight track of HALO is indicated by the blue line. The cloud retrieval is applied to the HALO flight segment for the leg between 08:15 UTC and 08:36 UTC (highlighted in red) when HALO did fly above the cirrus. During this period the aircraft flew constantly at 12.6 km height from South to North along $14°$ W. Due to low horizontal advection and hence slow cloud formation it can be expected that the Terra MODIS image (Fig. 12) actually reflects the cloud cover investigated by HALO. The cirrus developed along a warm conveyor belt and contained embedded contrails as indicated by the lidar backscatter profiles at λ = 1064 nm and λ = 532 nm of WALES (see Fig. 13). The time period for which τ is retrieved is marked by the black frame. The selected flight segment is characterized by a constant cloud top height and a slightly increasing cloud bottom height towards northern flight direction. While the upper most cloud top is relatively homogeneous, ~~the~~ there is significant variability in the layer below which is visible in the backscatter profile of WALES. The beginning of the black marked area shows high backscatter ratios of up to 500 indicating high reflectivity of a dense cirrus. At the end of the selected time period the backscatter decreases. The lower part of the cirrus shows small-scale variability mainly connected to sedimentation of ice crystals. ~~Figure 14(a)~~

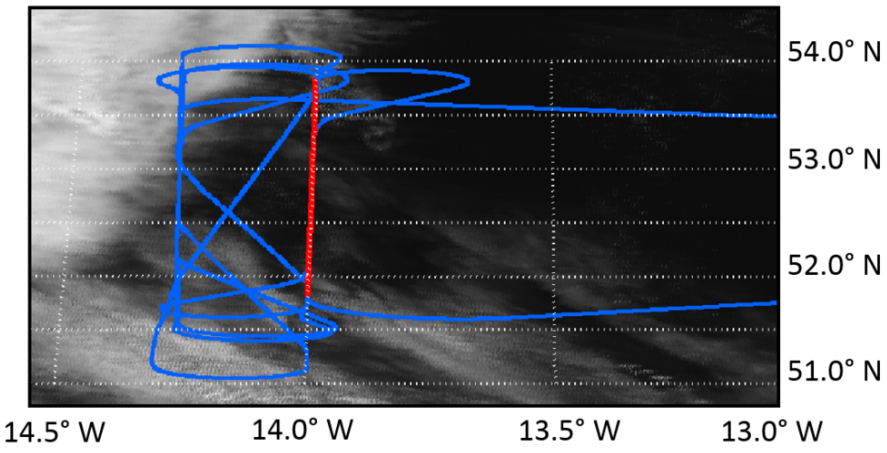

Figure 12. Investigated cloud field observed by MODIS-Terra on 26 March 2014. The flight track of HALO is indicated by the blue line. The flight leg between 08:15 UTC and 08:36 UTC for which the cirrus retrieval is performed is indicated by the red line.

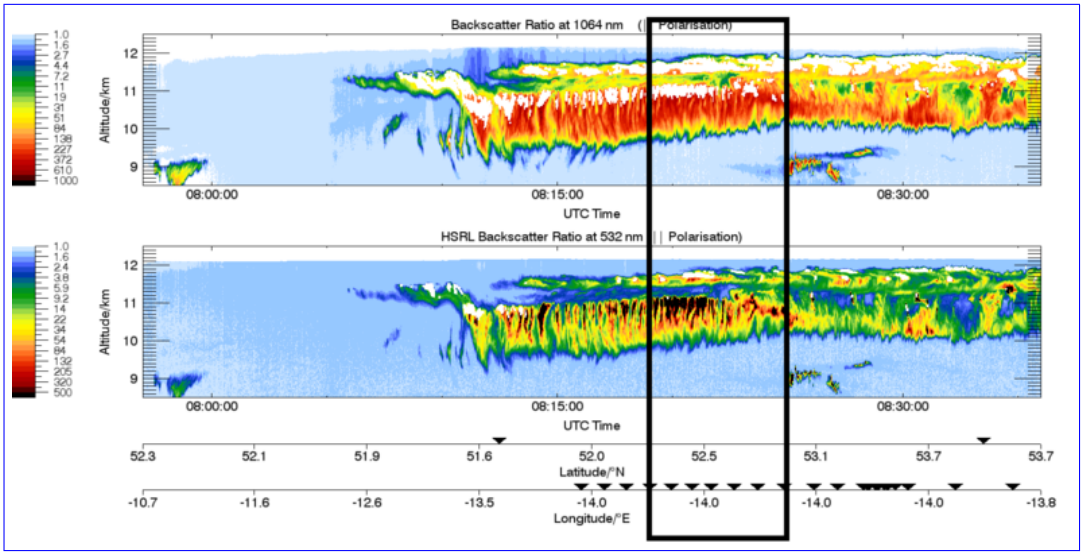

Figure 13. Vertical profiles of backscatter ratios at λ = 1064 nm (upper panel) and λ = 532 nm (lower panel) measured by WALES between 07:50 UTC and 08:50 UTC. The time period for which τ is retrieved is marked by the black rectangle.~~Areas which are influenced by a second cloud layer are highlighted by the red boxes.~~

5.2.1 Time series of cirrus optical thickness

Figure 14a shows a 20 minutes long flight segment of retrieved τ at λ = 532 nm calculated from SMART, mini-DOAS nadir and ~~scanning~~ sideward viewing spectrometers. WALES measurements are included for comparison. Along the analyzed cirrus, the retrieved τ ranges between 0.1 and 1.3 indicating the horizontal variability of the cirrus. The general decrease of τ towards

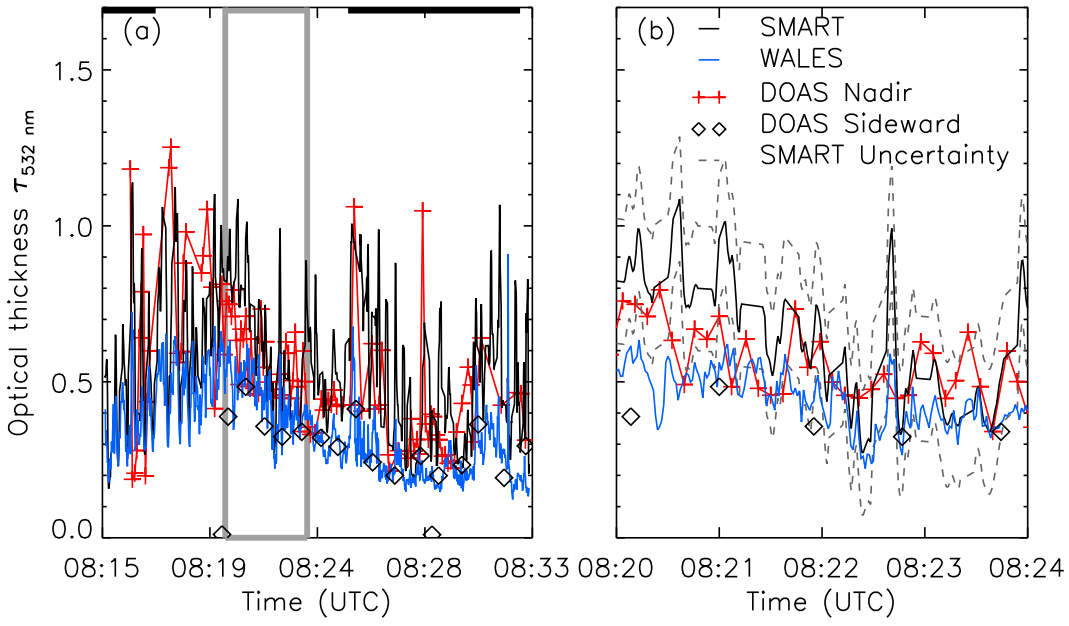

Figure 14. Time slices of the investigated flight segment on 26 March 2014 (a) and zoom (b) of τ at $\lambda = 532$ nm retrieved from SMART (black line), WALES (gray line), mini-DOAS ~~Off-nadir~~ sideward viewing (diamonds) and nadir spectrometers (crosses) along the flight track of ML-CIRRUS flight on 26 March 2014. ~~Sections~~ Periods with the second cloud layer are marked by the black lines at the top of (a).

higher latitudes (increasing time) matches with the cloud pattern observed by WALES. While SMART and mini-DOAS nadir channels resolve the cirrus variability observed by WALES, the ~~off-nadir~~ sideward viewing channel retrieval does not cover these fluctuations due to the reduced time resolution of the scanning mode and the large spatial scale (tenth of kilometers) over which ~~off-nadir~~ sideward viewing measurements average. At some locations, e.g. 08:21 UTC, τ retrieved by SMART and mini-DOAS significantly exceed the measurements of WALES. ~~In Fig. 13 these areas are highlighted in red. The first section ranges from 08:15 UTC until 08:17 UTC. The higher reflectivity as compared to the other parts of the flight leg is caused by ice crystals~~ Mostly likely both instruments retrieve larger τ than WALES since ice crystals were falling out of the cirrus ~~resulting in higher upward I. The~~ obscured to the Lidar measurements. A second segment with higher ~~reflectivity~~ retrieved τ is likely due to an underlying cirrus between 8.5 km and 9.5 km altitude ~~. The differences between SMART, mini-DOAS and WALES result from the detection of the second cloud layer by SMART and mini-DOAS, which is obscured for~~ that is also obscured to the detection by WALES. Therefore, a positive systematic offset of the retrieved τ occurs for SMART and mini-DOAS. These data points are excluded from the following analysis. Nevertheless, there is a slight chance that a few cloud fragments of these second cloud layers are still affecting the SMART- and mini-DOAS retrieval. Both passive sensors have a larger FOV compared to WALES and, therefore, are more likely sensitive to cloud layers located below the cirrus.

~~For the investigated time period the~~ Average τ are calculated for the filtered time period (indicated by the grey box in Fig. 14)

for each instrument. Due to different sampling intervals, a different resolution and number of observations are included in the averaging calculations. The retrieved average of τ at 532 nm is ~~0.54~~ 0.54 ± 0.2 (SMART), ~~0.49~~ 0.49 ± 0.2 (mini-DOAS nadir ~~spectrometers), 0.27~~ spectrometer), 0.27 ± 0.2 (mini-DOAS ~~scanning~~ sideward viewing spectrometer) and ~~0.32~~ 0.32 ± 0.02 (WALES). The ~~result indicate a general~~ results indicate a reasonable agreement of τ retrieved by SMART and mini-DOAS nadir channel, while lower τ are inferred from mini-DOAS ~~off-nadir~~ sideward viewing and WALES measurements. Taking the WALES measurements as a reference, the measurements of SMART and mini-DOAS overestimate τ. However, by estimating the uncertainty of the mini-DOAS and SMART basing on RTS, the measurement error of $I^{\mathrm{N}}_{\mathrm{S},1180}$ (~~10 %) indicates~~ $14.5\,\%$) by SMART results in an uncertainty range of retrieved τ of ± 0.2~~which is well within the~~ , which covers the values of τ obtained by WALES. The uncertainty range of ~~WALES. The~~ τ is determined by running the retrieval twice with a bias of measured $I^{\mathrm{N}}_{\mathrm{S},1180}$ with $\pm 14.5\,\%$ uncertainty at 1180 nm wavelength as upper and lower border. The resulting upper and lower retrieved τ represent the retrieval uncertainty. The mean τ inferred from the mini-DOAS ~~off-nadir~~ sideward viewing observations is significantly lower than measured by SMART and mini-DOAS nadir measurements. Differences in τ range up to ± 0.73 between SMART and mini-DOAS sideward viewing observations. This may result from ~~different field of view of the off-nadir~~ the different FOV of the sideward viewing geometry that does not observe the exact same clouds as SMART and nadir channels did. With the scanning sensors orientated to starboard the ~~off-nadir~~ sideward viewing retrieval corresponds to cirrus 8 km east of the flight track. As the MODIS satellite image in Fig. 12 indicates, the cirrus becomes slightly thinner towards east, which ~~agrees with~~ possibly is due to the lower values of τ~~provided by the~~ . Other potential reasons are the assumed ice crystal shapes for the RTS and different field-of-view of the passive and active remote sensing instruments. On the other hand, the agreement between mini-DOAS ~~off-nadir retrieval~~ sideward observations and WALES is significantly better. The maximum difference of τ between mini-DOAS sideward channels and WALES is ± 0.25 while the difference between the mean values is ± 0.05 ($15.6\,\%$). With WALES and mini-DOAS measuring in different viewing geometries but showing better agreement, the differences of τ retrieved by SMART is most likely caused by uncertainties in α. As discussed in Section 2.3, nadir observations are stronger affected by α than sideward observations. This is confirmed by the smaller differences between WALES and mini-DOAS sideward observations and indicates the advantage of the sideward viewing retrieval due to a reduced surface influence and lower retrieval uncertainty.

Figure 14~~(b)~~ b displays a zoom of the time series between 08:20 UTC to 08:24 UTC. During this flight segment, τ inferred by WALES is characterized by systematic oscillations varying between 0.2 and 1.1 also visible in the backscatter profile of WALES in Fig. 13. The lag time between two maxima is approximately between 20 s and 25 s flight time, which corresponds to a horizontal distance between 4.4 km and 5.5 km. This pattern is present in the measurements of SMART, WALES and the mini-DOAS nadir channels even though ~~a little bit~~ partly obscured in the latter measurements due to its reduced time ~~resolution. Overall the comparison provides evidence that the inferred τ agrees between the sensors.~~and space resolution.

Figure 15~~(a) and Fig. 15 (b)~~ a to d show scatter plots of retrieved τ for the different ~~instruments~~instrument combinations. A linear regression through the origin is performed and displayed in all cases. Data where a second cloud layer was present below the cirrus (gray points) are excluded. The comparison between SMART and WALES in Fig. 15~~(a)~~ a shows that the majority of the data is below the 1:1 line (gray). The linear regression results in $f(x) = 0.6621 \cdot x$. The regression confirms that SMART

systematically retrieves higher ~~values of~~ τ compared to WALES.~~The scattered data points lie below the regression and the majority of data are likely still contaminated by a second cloud layer (gray points) that effects the SMART retrieval but are not include in the WALES retrieval.~~

Compared to SMART, mini-DOAS nadir ~~spectrometers~~ observations of τ depart less from WALES (Fig. 15~~(b))~~b. Similar to SMART, the slope of the linear fit $f(x) = 0.6943 \cdot x$ indicates that mini-DOAS systematically overestimates τ compared to WALES. This similarity between SMART and mini-DOAS is obvious as SMART and mini-DOAS rely on the same radiometric calibration and retrieval. As indicated in Fig. 14b retrieved τ from WALES and the mini-DOAS sideward viewing channels agree well confirmed by the linear regression in Fig. 15c that gives a slope of $f(x) = 1.0328 \cdot x$ close to unity. The overestimation of retrieved τ by the mini-DOAS nadir channels compared to the sideward channels is visible in Fig. 14d which results in a linear fit of $f(x) = 1.642 \cdot x$.

5.3 ~~Probability distribution of cirrus optical thickness~~

~~For~~ Overall the comparison provides evidence that the inferred τ agrees between the different sensors.
Having nadir and sideward viewing observations at the same time allows to select the appropriate measurement geometry depending on cloud situation, e.g. τ and α. The sensitivity studies in Section 2.4 suggest that a combination of nadir and sideward viewing measurements allow a retrieval of τ for wide range of cirrus clouds depending on the observation conditions. For thin clouds the sideward viewing geometry would be preferred. In case the cloud becomes optically too thick, leading to high upward $I^{\mathrm{V}}_{\mathrm{S},1180}$ and a saturation of ε_τ, no retrievals of τ are possible. Then, switching to nadir observations of $I^{\mathrm{N}}_{\mathrm{S},1180}$ still enables to determine the amount of reflected radiation and to retrieve τ.

5.2.1 Probability distribution of cirrus optical thickness

For further comparison the ~~frequency of occurrence~~ probability density functions (PDF) of τ retrieved by SMART, mini-DOAS nadir spectrometers and WALES ~~is investigated. The PDFs~~ was investigated. A PDF of mini-DOAS sideward viewing spectrometers is not included because of the limited number of data points making a statistically meaningful PDF impossible. The PDF are shown in Fig. 16. Corresponding mean and median values of the distributions are given in Tab. 4. SMART (black solid line) and mini-DOAS (~~gray~~ red solid line) ~~almost show the same~~ which base on the same radiometric calibration and retrieval method show a comparable PDF indicating that both instruments measured the same cloud area. In both cases observed τ range from 0.15 to 1.25 for SMART and mini-DOAS and from 0.15 to 0.7 for WALES (black dashed line). The PDF maxima for SMART and mini-DOAS is around $\tau = 0.4$, slightly more pronounced for the mini-DOAS. For ~~both instruments, the PDFs are squeed~~ SMART and mini-DOAS, the PDF are skewed to small τ with a median of 0.47 for SMART and 0.48 for mini-DOAS. ~~It~~ This is slightly smaller than the mean value of 0.5 for SMART and 0.51 for mini-DOAS. Both ~~PDFs~~ PDF are long-tailed towards large τ, slowly decreasing to higher values of τ. In contrast, τ measured by WALES (black dashed line) shows a stronger shift to low τ as the mean value of τ is significantly lower. The most frequent τ ~~was around $\tau = 0.2$~~is around 0.2. The WALES measurement do not show τ larger than 0.7~~what~~. This results in a stronger decrease of ~~of~~ the WALES PDF to

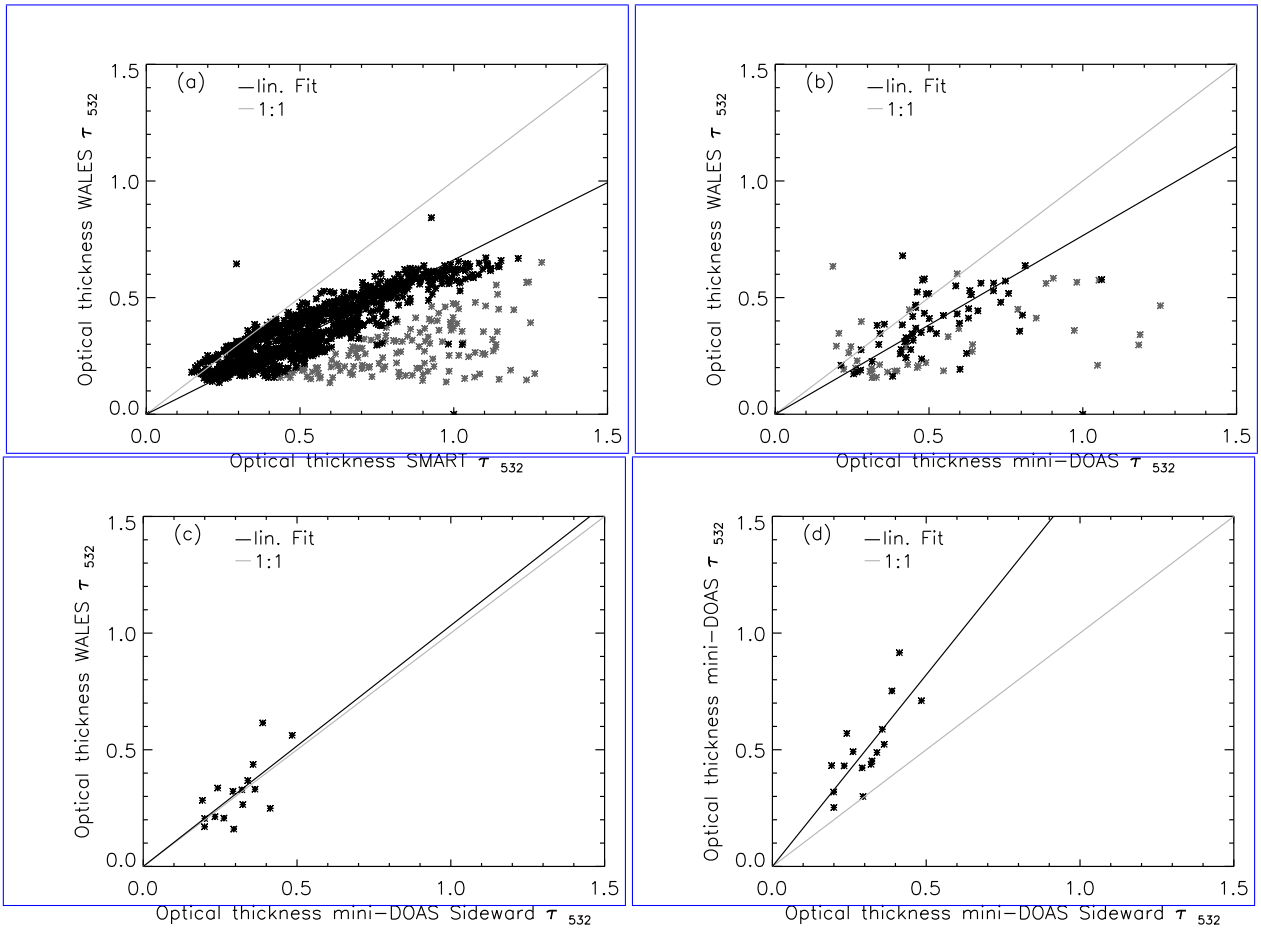

Figure 15. (a) Comparison of the retrieved cirrus optical thickness τ by WALES and SMART at $\lambda = 532$ nm wavelength. (b) Comparison of the retrieved cirrus optical thickness τ by WALES and mini-DOAS nadir channel at $\lambda = 532$ nm wavelength. Measurements when a second cirrus layer was present are displayed in grey and are discarded in the regression. (c) Comparison of the retrieved cirrus optical thickness τ by WALES and mini-DOAS sideward viewing channels at $\lambda = 532$ nm wavelength. No data is discarded. (d) Comparison of the retrieved cirrus optical thickness τ by mini-DOAS nadir and sideward viewing channels at $\lambda = 532$ nm wavelength.

higher τ compared to SMART and mini-DOAS. The difference may be explained by different ~~field of view~~ FOV and therefore measuring different horizontal parts of the clouds. It is assumed, that SMART and mini-DOAS, e.g. due to similar large FOV, ~~measure additional scattered radiation~~ average over larger areas and are influenced by ~~three dimensional~~ 3-D radiative effects caused by clouds, atmosphere and surface, which are not considered in the presented ~~1-dimensional~~ 1-D RTS and the iterative retrieval (Davis et al., 1997). Contrarily WALES has a more narrow FOV resulting from an opening angle of the telescope of 0.08°. Because of the smaller FOV of WALES the spot of the laser at cloud top covers a smaller area compared to SMART and mini-DOAS which have a spatial resolution in the range of tenth of meters depending on the distance between aircraft and cloud top. Therefore, WALES resolves finer cloud structures that may exhibit lower τ (cloud gaps) or larger τ. In case of the

Table 4. Mean and median of the PDFs of cirrus optical thickness τ derived from WALES, SMART and mini-DOAS.

	mean	median
WALES	0.35	0.33
SMART	0.56	0.52
mini-DOAS	0.52	0.47

most unfortunate situation WALES would measure a cloud free region but SMART and mini-DOAS receive I^N from a much larger area including clouds with various τ. This better spatial resolution of WALES to SMART and mini-DOAS may explain the shift of WALES to lower τ but does not give reasons for the lower amount of high τ.~~Differences in~~

Differences in the PDF of τ may also result from the measurement methodologies. While WALES uses a laser with small FOV for active remote sensing~~with a laser~~, SMART and mini-DOAS are passive remote instruments relaying on scattered sunlight. Therefore, SMART and mini-DOAS are influenced by the ~~RT~~ RTS of the whole atmosphere, while WALES is only sensitive to scattering within its narrow LOS. Additionally, the ~~vertical probing of the cloud also depends on the used wavelength~~ different wavelengths of the measurements may introduce biases in the retrieved τ due to different penetration depth of the reflected radiation into the cloud (Platnick, 2000). Therefore, the wavelength selection defines the layer in the cloud which is probed. While WALES uses backscatter measurements at λ = 532 nm and λ = 1064 nm the ~~retrieval~~ measurements of $I_{S,1180}$ by SMART and mini-DOAS ~~is~~ are performed at λ = 1180 nm. Although the retrieval accounts for the wavelength dependence of scattering, absorption and refraction on ice crystals (Takano and Liou, 1989; Yang et al., 2013) by scaling the retrieved τ at λ = 1180 nm to λ = 532 nm to make it comparable between the different instruments.

Referring to the sensitivity studies from Section 2 the influence of α and the ice crystal shape effects on the upward I measured in nadir geometry is larger compared to the sideward viewing measurements. While nadir observations, especially of optical thin clouds, are strongly influenced by α, sideward viewing observations are less effected. This is demonstrated in this case study where the sea surface albedo may vary due to different surface wind speeds (Cox and Munk, 1954) and indicates the advantage of sideward viewing measurements. An other possible reason for the differences in the PDF and the mean values between mini-DOAS nadir and sideward retrievals of τ are the varying angular dependencies of measured I for different ice crystal shapes. For the RTS in the retrieval an assumption for the ice crystal shape has to be made which slightly influences the result for the nadir retrieval. This is more pronounced for the retrieval using the sideward channels of the mini-DOAS which is presented in the sensitivity study in Section 2.2. The WALES measurements are less effect by different ice crystal shapes but more on the ice crystal size assumption which is a general difference between the active and remote sensing instruments presented here.

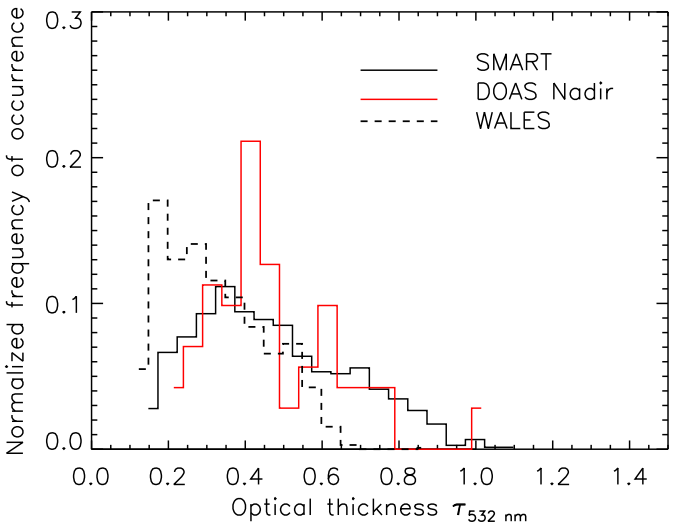

Figure 16. PDFs of cirrus optical thickness τ at $\lambda = 532$ nm retrieved from SMART, mini-DOAS and WALES ~~measurement~~measurements. The bin size is 0.05 units of τ.

6 Conclusions

The potential of airborne spectral radiance measurements in ~~off-nadir~~ sideward viewing direction for cirrus remote sensing is investigated. For this purpose ~~RTS~~ radiative transfer simulations (RTS) are performed and airborne measurements of the Spectral Modular Airborne Radiation measurement sysTem (SMART) and the Differential Optical Absorption Spectrometer (mini-DOAS) are compared. A sensitivity study based on RTS showed that ~~off-nadir~~ sideward viewing measurements are generally more suited for detecting and investigating optically thin cirrus ~~and SVC~~ than observations in nadir orientation. Using ~~off-nadir~~ sideward viewing observations the sensitivity ~~of measured upward radiance I^{L}~~ ε_τ of measured radiance I^{V} is larger than for nadir measurements up to a factor of ~~10~~ ten depending on the ~~details of the~~ selected observation geometry and cloud properties. For cirrus optical thickness $\tau \leq 1$ and all simulated sideward vieweing geometries ε_τ is larger compared to nadir observations. This results in a higher retrieval accuracy due to a reduced influence of measurement uncertainties. The RTS indicate that large observation angles θ_{L} θ_{V} (close to the horizon) and small relative solar azimuth angle ϕ (observations in direction of the Sun) result in ~~the highest sensitivity.Additionally, the smoothing of horizontal variability of optical thickness-fields by off-nadir observations has also been shown.~~highest ε_τ.

For retrievals of ~~cirrus optical thickness~~ τ using ~~off-nadir~~ sideward viewing measurements, the wavelength selection is crucial. Simulations indicate that ~~wavelength~~ wavelengths larger than $\lambda = 900$ nm are best suited. ~~While reflected I^{L} of smaller wavelength~~ Reflected I^{V} of smaller wavelengths is significantly contaminated by scattering and absorption due to ~~atmospheric molecules~~the reducing interference from Rayleigh scattering. Furthermore, the ~~off-nadir~~ sideward viewing orientation reduces the influence of the surface albedo α on reflected ~~I^{L}.~~ I^{V}. As a result, a precise assumption of α in the retrieval algorithm is less

crucial. This substantially improves the uncertainties of passive solar remote sensing especially in locations of highly variable α, where an exact assumption of α is impossible.

~~Similarly,~~ Contrarily, for sideward observations, a reasonable good assumption of the ice crystal shape used in the RTS is important. ~~In off-nadir~~ The RTS showed that in sideward viewing geometry the shape effects on reflected ~~I^{L}~~ I^{V} are more pronounced than for nadir measurements. An incorrect assumption ~~will~~ would bias the retrieval of τ significantly. On the other hand, the sensitivity for different ice crystal shapes may offer the possibility to retrieve shape information when measuring at different viewing angles. Nevertheless, smoothing of horizontal variability of optical thickness-fields by sideward viewing observations has to be taken into account.

~~In order to apply a radiance based cloud retrieval to off-nadir measurements of mini-DOAS during ML-CIRRUS, the raw measurements are radiometrically calibrated. For this purpose a cross-calibration between SMART and mini-DOAS nadir and off-nadir channels is performed to calculate calibrated I_{mD} from mini-DOAS raw counts. A comparison of ML-CIRRUS measurements shows that calibrated upward I_{mD} of mini-DOAS is within the uncertainty range of SMART. Individual cross-calibrations from different campaigns and flights revealed, that the calibrations can be transferred to different flights within one campaign providing that no technical adjustments are performed.However, considering the uncertainty and limitations of such cross-calibrations, a laboratory radiometric calibration of the mini-DOAS is recommended to improve the uncertainties of the cloud retrieval and to allow measurements independent to SMART.~~Using the SMART, mini-DOAS nadir and ~~scanning sensor~~ sideward measurements in conjunction with an iterative retrieval, τ is derived for a case study of ML-CIRRUS. ~~For individual retrieval, the~~ The inferred τ from SMART, mini-DOAS and the additional lidar measurement by the Water Vapour Lidar Experiment in Space (WALES) show a reasonable good agreement in τ for the nadir channels with absolute differences of ± 0.22 ($66.6\,\%$) between SMART and WALES and ± 0.17 ($52.3\,\%$) between mini-DOAS and WALES observations respectively. The retrieval using mini-DOAS ~~scanning~~ sideward channels is also successful demonstrated for a reduced set of observations limited to ~~θ_{L}~~ θ_{V} between $85°$ and $90°$. Differences in τ range up to ± 0.73 between SMART and mini-DOAS ~~off-nadir observations are~~ sideward viewing observations and are partly caused by the different viewing geometries. ~~While the scanning~~ First, the sideward telescopes view into starboard direction~~thus~~, probing the cirrus cloud top at approximately 8000 m aside the flight track. ~~However, the case study shows that cirrus retrieval using airborne off-nadir observations with~~ Second, the nadir observations may suffer from uncertainties in α while the sideward observations are less effected by changes in α. Even for sea surfaces as presented here, α may change due to different wind speeds. Other potential reasons are the assumed ice crystal shapes in the RTS and different field-of-view of the passive and active remote sensing instruments. This conclusion is apparent from different probability distributions. While SMART and mini-DOAS ~~are possible and can increase the potential of remote sensing on HALO.~~ show a median around $\tau = 0.4$, the median for WALES is shifted to lower τ around 0.2, indicating that WALES observed small τ more frequently. The difference of mean values of τ between mini-DOAS sideward channels and WALES is smaller with ± 0.05 ($15.6\,\%$). This shows the advantage of the sideward viewing retrieval due to a reduced surface influence and lower retrieval uncertainty, because of high ε_{τ} compared to the nadir measurements. For future dedicated cloud observations it is recommended to adjust ~~θ_{L}~~ θ_{V} to the most sensitive direction between $60°$ and $90°$ to reduce the uncertainty in the ~~off-nadir~~ sideward viewing retrieval. Additional ~~off-nadir~~ sideward viewing scans in homogeneous cloud conditions might be

used to estimate the cirrus ice crystal shape and minimize the retrieval uncertainties. The case study shows that cirrus retrieval using airborne sideward viewing observations with mini-DOAS are possible and can increase the potential of remote sensing on HALO significantly. Therefore, we suggest sideward viewing measurements for passive remote sensing of optically thin cirrus clouds.

Acknowledgements. This research was funded by the German Research Foundation (DFG, HALO-SPP 1294). The authors acknowledge the support by the Deutsche Forschungsgemeinschaft (DFG) through grants PF 384/7-1/2, PF 384/16-1 and WE 1900/35-1. The authors thank the pilots and appreciate the support by the Flugbereitschaft of the German Aerospace Center (DLR). Additionally the authors thank enviscope GmbH for preparation and testing of SMART.

References

Abrams, M. C., Chang, A. Y., Gunson, M. R., Abbas, M. M., Goldman, A., Irion, F. W., Michelson, H. A., Newchurch, M. J., Rinsland, C. P., Stiller, G. P., and Zander, R.: On the assessment and uncertainty of atmospheric trace gas burden measurements with high resolution infrared solar occultation spectra from space by the ATMOS Experiment, Geophys. Res. Lett., 23, 2337–2340, doi:10.1029/96GL01794, 1996.

Baum, B. A., Heymsfield, A. J., Yang, P., and Bedka, S. T.: Bulk scattering properties for the remote sensing of ice clouds. Part I: Microphysical data and models, J. Appl. Meteor., 44, 1885–1895, 2005.

Bierwirth, E., Wendisch, M., Ehrlich, A., Heese, B., Tesche, M., Althausen, D., Schladitz, A., Müller, D., Otto, S., Trautmann, T., Dinter, T., von Hoyningen-Huene, W., and Kahn, R.: Spectral surface albedo over Morocco and its impact on the radiative forcing of Saharan dust, Tellus, 61B, 252–269, 2009.

Bierwirth, E., Wendisch, M., Jakel, E., Ehrlich, A., Schmidt, K. S., Stark, H., Pilewskie, P., Esselborn, M., Gobbi, G. P., Ferrare, R., Muller, T., and Clarke, A.: A new method to retrieve the aerosol layer absorption coefficient from airborne flux density and actinic radiation measurements RID E-7433-2010, J. Geophys. Res., 115, D14 211, doi:10.1029/2009JD013636, 2010.

Bourassa, A. E., Degenstein, D. A., and Llewellyn, E. J.: Climatology of the subvisual cirrus clouds as seen by OSIRIS on Odin, Adv. Space Res., 36, 807–812, doi:http://dx.doi.org/10.1016/j.asr.2005.05.045, 2005.

Bozzo, A., Maestri, T., Rizzi, R., and Tosi, E.: Parameterization of single scattering properties of mid-latitude cirrus clouds for fast radiative transfer models using particle mixtures, Geophys. Res. Lett., 35, L16 809, 2008.

Brückner, M., Pospichal, B., Macke, A., and Wendisch, M.: A new multispectral cloud retrieval method for ship-based solar transmissivity measurements, J. Geophys. Res. Atmos., 119, 11.338–11.354, doi:10.1002/2014JD021775, 2014.

Chen, T., Rossow, W., and Zhang, Y.: Radiative effects of cloud-type variations, J. Climate, 13, 264–286, 2000.

Clark, R. N., Swayze, G. A., Wise, R., Livo, E., Hoefen, T., Kokaly, R., and Sutley, S. J.: USGS digital spectral library splib06a, Tech. rep., U.S. Geological Survey, http://speclab.cr.usgs.gov/spectral-lib.html, 2007.

Clerbaux, C., Hadji-Lazaro, J., Turquety, S., Mégie, G., and Coheur, P.-F.: Trace gas measurements from infrared satellite for chemistry and climate applications, Atmos. Chem. Phys., 3, 1495–1508, doi:10.5194/acp-3-1495-2003, 2003.

Comstock, J. M., Ackerman, T. P., and Mace, G. G.: Ground-based lidar and radar remote sensing of tropical cirrus clouds at Nauru Island: Cloud statistics and radiative impacts, J. Geophys. Res., 107, 4714, doi:10.1029/2002JD002203, 2002.

Cox, C. and Munk, W.: Measurement of the roughness of the sea surface from photographs of the sun's glitter, J. Opt. Soc. Am. A., 44, 838–850, 1954.

Cziczo, D. J., Froyd, K. D., Hoose, C., Jensen, E. J., Diao, M., Zondlo, M. A., Smith, J. B., Twohy, C. H., and Murphy, D. M.: Clarifying the Dominant Sources and Mechanisms of Cirrus Cloud Formation, Science, doi:10.1126/science.1234145, 2013.

Davis, A., Marshak, A., Cahalan, R., and Wiscombe, W.: The Landsat scale break in stratocumulus as a three-dimensional radiative transfer effect: Implications for cloud remote sensing, J. Atmos. Sci., 54, 241–260, 1997.

Davis, S., Hlavka, D., Jensen, E., Rosenlof, K., Yang, Q. O., Schmidt, S., Borrmann, S., Frey, W., Lawson, P., Voemel, H., and Bui, T. P.: In situ and lidar observations of tropopause subvisible cirrus clouds during TC4, J. Geophys. Res., 115, D00J17, doi:10.1029/2009JD013093, 2010.

Delanoe, J., Protat, A., Jourdan, O., Pelon, J., Papazzoni, M., Dupuy, R., Gayet, J.-F., and Jouan, C.: Comparison of Airborne In Situ, Airborne Radar-Lidar, and Spaceborne Radar-Lidar Retrievals of Polar Ice Cloud Properties Sampled during the POLARCAT Campaign, J. Atmos. Oceanic Technol., 30, 57–73, doi:10.1175/JTECH-D-11-00200.1, 2013.

Ehret, G., Gross, S., Schäfler, A., Wirth, M., Fix, A., and Kiemle, C.: Characterization of Cirrus Cloud Properties by Airborne Differential Absorption and High Spectral Resolution Lidar Measurements, AGU Fall Meeting Abstracts, 2014.

Ehrlich, A., Bierwirth, E., Wendisch, M., Gayet, J.-F., Mioche, G., Lampert, A., and Heintzenberg, J.: Cloud phase identification of Arctic boundary-layer clouds from airborne spectral reflection measurements: Test of three approaches, Atmos. Chem. Phys., 8, 7493–7505, 2008.

Eichler, H., Ehrlich, A., Wendisch, M., Mioche, G., Gayet, J.-F., Wirth, M., Emde, C., and Minikin, A.: Influence of ice crystal shape on retrieval of cirrus optical thickness and effective radius: A case study, J. Geophys. Res., 114, D19203, doi:doi:10.1029/2009JD012215, 2009.

Eloranta, E. W.: Practical model for the calculation of multiply scattered lidar returns, Appl. Opt., 37, 2464–2472, doi:10.1364/AO.37.002464, 1998.

Esselborn, M., Wirth, M., Fix, A., Tesche, M., and Ehret, G.: Airborne high spectral resolution lidar for measuring aerosol extinction and backscatter coefficients, Appl. Opt., 47, 346–358, doi:10.1364/AO.47.000346, 2008.

Frey, W., Borrmann, S., Kunkel, D., Weigel, R., de Reus, M., Schlager, H., Roiger, A., Voigt, C., Hoor, P., Curtius, J., Krämer, M., Schiller, C., Volk, C. M., Homan, C. D., Fierli, F., Di Donfrancesco, G., Ulanovsky, A., Ravegnani, F., Sitnikov, N. M., Viciani, S., D'Amato, F., Shur, G. N., Belyaev, G. V., Law, K. S., and Cairo, F.: In situ measurements of tropical cloud properties in the West African Monsoon: upper tropospheric ice clouds, Mesoscale Convective System outflow, and subvisual cirrus, Atmos. Chem. Phys., 11, 5569–5590, doi:10.5194/acp-11-5569-2011, http://www.atmos-chem-phys.net/11/5569/2011/, 2011.

Fricke, C., Ehrlich, A., Jäkel, E., Bohn, B., Wirth, M., and Wendisch, M.: Influence of local surface albedo variability and ice crystal shape on passive remote sensing of thin cirrus, Atmos. Chem. Phys., 14, 1943–1958, doi:10.5194/acp-14-1943-2014, 2014.

Froyd, K. D., Murphy, D. M., Lawson, P., Baumgardner, D., and Herman, R. L.: Aerosols that form subvisible cirrus at the tropical tropopause, Atmos. Chem. Phys., 10, 209–218, doi:10.5194/acp-10-209-2010, 2010.

Fu, Q. and Liou, K.: Parameterization of the radiative properties of cirrus clouds, J. Atmos. Sci., 50, 2008–2025, 1993.

Fu, Q., Hu, Y., and Yang, Q.: Identifying the top of the tropical tropopause layer from vertical mass flux analysis and CALIPSO lidar cloud observations, Geophys. Res. Lett., 34, doi:10.1029/2007GL030099, l14813, 2007.

Gross, S., Forster, L., Wirth, M., Schäfler, A., Freudenthaler, V., Fix, A., and Mayer, B.: Characterization of mid-latitude cirrus cloud with airborne and ground-based lidar measurements during ML-CIRRUS, in: EGU General Assembly Conference Abstracts, vol. 17 of *EGU General Assembly Conference Abstracts*, p. 10283, 2015.

Gueymard, C. A.: The sun's total and spectral irradiance for solar energy applications and solar radiation models, Solar Energy, 76, 423–453, 2004.

Hüneke, T.: Aufbau und Charakterisierung eines sechsfach–miniDOAS–Spektrographen für das Forschungsflugzeug DLR-HALO, Master's thesis, Ruprecht-Karls-University Heidelberg, 2011.

Hüneke, T., Aderhold, O.-A., Bounin, J., Dorf, M., Gentry, E., Grossmann, K., Groß, J.-U., Hoor, P., Joeckel, P., Kenntner, M., Knecht, M., Knapp, M., Lörks, D., Ludmann, S., Raecke, R., Reichert, M., Schulte, I., Schwab, F., Weimar, J., Werner, B., Zahn, A., Ziereis, H., and Pfeilsticker, K.: The novel HALO mini-DOAS instrument: Inferring trace gas concentrations from air-borne UV/visible limb spectroscopy under all skies using the scaling method, Atmos. Meas. Tech, in prep., 2017.

IPCC: Climate Change 2013: The Physical Science Basis, Cambridge University Press, 2013.

Jensen, E. J., Pfister, L., Jordan, D. E., Bui, T. V., Ueyama, R., Singh, H. B., Thornberry, T., Rollins, A. W., Gao, R.-S., Fahey, D. W., Rosenlof, K. H., Elkins, J. W., Diskin, G. S., DiGangi, J. P., Lawson, R. P., Woods, S., Atlas, E. L., Rodriguez, M. A. N., Wofsy, S. C., Pittman, J., Bardeen, C. G., Toon, O. B., Kindel, B. C., Newman, P. A., McGill, M. J., Hlavka, D. L., Lait, L. R., Schoeberl, M. R., Bergman, J. W., Selkirk, H. B., Alexander, M. J., Kim, J.-E., Lim, B. H., Stutz, J., and Pfeilsticker, K.: The NASA Airborne Tropical TRopopause EXperiment (ATTREX): High-Altitude Aircraft Measurements in the Tropical Western Pacific, BAMS, doi:10.1175/BAMS-D-14-00263.1, http://dx.doi.org/10.1175/BAMS-D-14-00263.1, 2015.

Kärcher, B.: Properties of subvisible cirrus clouds formed by homogeneous freezing, Atmos. Chem. Phys., 2, 161–170, doi:10.5194/acp-2-161-2002, 2002.

King, M. D., Platnick, S., Yang, P., Arnold, G. T., Gray, M. A., Riedi, J. C., Ackerman, S. A., and Liou, K. N.: Remote sensing of liquid water and ice cloud optical thickness and effective radius in the Arctic: Application of airborne multispectral MAS data, J. Atmos. Oceanic Technol., 21, 857–875, 2004.

Klepp, C., Ament, S., Bakan, S., Hirsch, L., and Stevens, B.: NARVAL Campaign Report, vol. 164, Reports on Earth System Science, Max Planck Institute for Meteorology Hamburg, Germany, 2014.

Lampert, A., Ehrlich, A., Dörnbrack, A., Jourdan, O., Gayet, J.-F., Mioche, G., Shcherbakov, V., Ritter, C., and Wendisch, M.: Microphysical and radiative characterization of a subvisible midlevel Arctic ice cloud by airborne observations - a case study, Atmos. Chem. Phys., 9, 2647–2661, 2009.

Lee, J., Yang, P., Dessler, A. E., Gao, B.-C., and Platnick, S.: Distribution and radiative forcing of tropical thin cirrus clouds, J. Atmos. Sci., 66, 3721–3731, doi:10.1175/2009JAS3183.1, 2009.

Mayer, B. and Kylling, A.: Technical note: The *libRadtran* software package for radiative transfer calculations - description and examples of use, Atmos. Chem. Phys., 5, 1855–1877, 2005.

McFarquhar, G. M., Heymsfield, A. J., Spinhirne, J., and Hart, B.: Thin and subvisual tropopause tropical cirrus: Observations and radiative impacts, J. Atmos. Sci., 57, 1841–1853, doi:10.1175/1520-0469(2000)057, 2000.

Nakajima, T. and King, M.: Determination of the optical thickness and effective particle radius of clouds from reflected solar radiation measurements. Part I: Theory, J. Atmos. Sci., 47, 1878–1893, 1990.

Oikarinen, L.: Effect of surface albedo variations on UV-visible limb-scattering measurements of the atmosphere, J. Geophys. Res., doi:10.1029/2001JD001492, 2002.

Ou, S., Liou, K., Gooch, W., and Takano, Y.: Remote sensing of cirrus cloud parameters using advanced very-high-resolution radiometer 3.7- and 10.9-μm channels, Appl. Opt., 32, 2171–2180, 1993.

Ou, S., Liou, K.-N., Takano, Y., Rao, X., Fu, Q., Heymsfield, A., Miloshevich, L., Baum, B., and Kinne, S.: Remote sounding of cirrus cloud optical depths and ice crystal structures from AVHRR data: Verification using FIRE II IFO measurements, J. Atmos. Sci., 52, 4143–4158, 1995.

Pierluissi, J. and Peng, G.-S.: New molecular transmission band models for LOWTRAN, Opt. Eng., 24, 541–547, 1985.

Platnick, S.: Vertical photon transport in cloud remote sensing problems, J. Geophys. Res., 105, 22 919–22 935, 2000.

Platt, C.: Remote sounding of high clouds. III: Monte Carlo calculations of multiple-scattered lidar returns, J. Atmos. Sci., 38, 156–167, 1981.

Platt, U. and Stutz, J.: Differential Optical Absorption Spectroscopy: Principles and Applications, Series: Physics of Earth and Space Environments, Springer Verlag, ISBN: 3540211934, 2008.

Pruppacher, H. and Klett, J.: Microphysics of Clouds and Precipitation, Kluwer Academic, 1997.

Rolland, P. and Liou, K.: Surface variability effects on the remote sensing of thin cirrus optical and microphysical properties, J. Geophys. Res., 106, 22 965–22 977, doi:10.1029/2001JD900160, 2001.

Rolland, P., Liou, K., King, M., Tsay, S., and McFarquhar, G.: Remote sensing of optical and microphysical properties of cirrus clouds using Moderate-Resolution Imaging Spectroradiometer channels: Methodology and sensitivity to physical assumptions, J. Geophys. Res., 105, 11 721–11 738, doi:10.1029/2000JD900028, 2000.

Sassen, K., Wang, Z., and Liu, D.: Cirrus clouds and deep convection in the tropics: Insights from CALIPSO and CloudSat, J. Geophys. Res. Atmos., 114, doi:10.1029/2009JD011916, 2009.

Sausen, R., Isaksen, I., Grewe, V., Hauglustaine, D., Lee, D., Myhre, G., Köhler, M., Pitari, G., Schumann, U., Stordal, F., and Zerefos, C.: Aviation radiative forcing in 2000: An update on IPCC (1999), Meteor. Z., 14, 555–561, 2005.

Schäfer, M., Bierwirth, E., Ehrlich, A., Heyner, F., and Wendisch, M.: Retrieval of cirrus optical thickness and assessment of ice crystal shape from ground-based imaging spectrometry, Atmos. Meas. Tech., 6, 1855–1868, doi:10.5194/amt-6-1855-2013, 2013.

Sen, P. K.: Estimates of the Regression Coefficient Based on Kendall's Tau, J. Am. Stat. Assoc., 63, 1379–1389, doi:10.1080/01621459.1968.10480934, 1968.

Shettle, E.: Models of aerosols, clouds and precipitation for atmospheric propagation studies, in: Atmospheric propagation in the uv, visible, ir and mm-region and related system aspects, no. 454 in AGARD Conference Proceedings, 1989.

Stamnes, K., Tsay, S.-C., Wiscombe, W., and Laszlo, I.: DISORT, a General-Purpose Fortran Program for Discrete-Ordinate-Method Radiative Transfer in Scattering and Emitting Layered Media: Documentation of Methodology, Tech. rep., Dept. of Physics and Engineering Physics, Stevens Institute of Technology, Hoboken, NJ 07030, 2000.

Takano, Y. and Liou, K.-N.: Solar radiative transfer in cirrus clouds. Part I: Single-scattering and optical properties of hexagonal ice crystals, J. Atmos. Sci., 46, 1–19, 1989.

Theil, H.: A Rank–Invariant Method of Linear and Polynomial Regression Analysis, in: Henri Theils Contributions to Economics and Econometrics, edited by Raj, B. and Koerts, J., vol. 23 of *Adv. S. Theo. App. Eco.*, pp. 345–381, Springer Netherlands, doi:10.1007/978-94-011-2546-8_20, 1992.

Toon, O. B., Starr, D. O., Jensen, E. J., Newman, P. A., Platnick, S., Schoeberl, M. R., Wennberg, P. O., Wofsy, S. C., Kurylo, M. J., Maring, H., Jucks, K. W., Craig, M. S., Vasques, M. F., Pfister, L., Rosenlof, K. H., Selkirk, H. B., Colarco, P. R., Kawa, S. R., Mace, G. G., Minnis, P., and Pickering, K. E.: Planning, implementation, and first results of the Tropical Composition, Cloud and Climate Coupling Experiment (TC4), J. Geophys. Res. Atmos., 115, doi:10.1029/2009JD013073, 2010.

Twomey, S. and Seton, K. J.: Inferences of gross microphysical properties of clouds from spectral reflectance measurements, J. Atmos. Sci., 37, 1065–1069, 1980.

Voigt, C., Schumann, U., Jurkat, T., Schäuble, D., Schlager, H., Petzold, A., Gayet, J.-F., Krämer, M., Schneider, J., Borrmann, S., Schmale, J., Jessberger, P., Hamburger, T., Lichtenstern, M., Scheibe, M., Gourbeyre, C., Meyer, J., Kübbeler, M., Frey, W., Eichler, H., Butler, T., Lawrence, M. G., Holzäpfel, F., Arnold, F., Wendisch, M., Döpelheuer, A., Gottschaldt, K., Baumann, R., Zöger, M., Sölch, I., Rautenhaus, M., and Dörnbrack, A.: In situ observations of young contrails- overview and selected results from the CONCERT campaign, Atmospheric Chemistry and Physics Discussions, 10, 12 713–12 763, doi:10.5194/acpd-10-12713-2010, http://www.atmos-chem-phys-discuss.net/10/12713/2010/, 2010.

Voigt, C., Schumann, U., Minikin, A., Abdelmonem, A., Afchine, A., Borrmann, S., Boettcher, M., Buchholz, B., Bugliaro, L., Costa, A., Curtius, J., Dollner, M., Dörnbrack, A., Dreiling, V., Ebert, V., Ehrlich, A., Fix, A., Forster, L., Frank, F., Fütterer, D., Giez, A., Graf,

K., Grooß, J.-U., Groß, S., Heimerl, K., Heinold, B., Hüneke, T., Järvinen, E., Jurkat, T., Kaufmann, S., Kenntner, M., Klingebiel, M., Klimach, T., Kohl, R., Krämer, M., Krisna, T. C., Luebke, A., Mayer, M., Mertes, S., Molleker, S., Petzold, A., Pfeilsticker, K., Port, M., Rapp, M., Reutter, P., Rolf, C., Rose, D., Sauer, D., Schäfler, A., Schlage, R., Schnaiter, M., Schneider, J., Spelten, N., Spichtinger, P., Stock, P., Walser, A., Weigel, R., Weinzierl, B., Wendisch, M., Werner, F., Wernli, H., Wirth, M., Zahn, A., Ziereis, H., and Zöger, M.: ML-CIRRUS – The airborne experiment on natural cirrus and contrail cirrus with the high-altitude long-range research aircraft HALO, Bulletin of the American Meteorological Society, doi:10.1175/BAMS-D-15-00213.1, 2016.

Wang, P.-H., Minnis, P., McCormick, M. P., Kent, G. S., and Skeens, K. M.: A 6–year climatology of cloud occurrence frequency from Stratospheric Aerosol and Gas Experiment II observations (1985–1990), J. Geophys. Res. Atmos., 101, 29 407–29 429, doi:10.1029/96JD01780, http://dx.doi.org/10.1029/96JD01780, 1996.

Wendisch, M., Müller, D., Schell, D., and Heintzenberg, J.: An airborne spectral albedometer with active horizontal stabilization, J. Atmos. Oceanic Technol., 18, 1856–1866, 2001.

Wendisch, M., Pilewskie, P., Pommier, J., Howard, S., Yang, P., Heymsfield, A. J., Schmitt, C. G., Baumgardner, D., and Mayer, B.: Impact of cirrus crystal shape on solar spectral irradiance: A case study for subtropical cirrus, J. Geophys. Res., 110, Art. No. D03 202, 2005.

Wendisch, M., Yang, P., and Pilewskie, P.: Effects of ice crystal habit on thermal infrared radiative properties and forcing of cirrus, J. Geophys. Res., 112, D03 202, doi:10.1029/2006JD007899, 2007.

Wendisch, M., Pöschl, U., Andreae, M. O., Machado, L. A. T., Albrecht, R., Schlager, H., Rosenfeld, D., Martin, S. T., Abdelmonem, A., Afchine, A., Araujo, A., Artaxo, R., Aufmhoff, H., Barbosa, H. M. J., Borrmann, S., Braga, R., Buchholz, B., Cecchini, M. A., Costa, A., Curtius, J., Dollner, M., Dorf, M., Dreiling, V., Ebert, V., Ehrlich, A., Ewald, F., Fisch, G., Fix, A., Frank, F., Fütterer, D., Heckl, C., Heidelberg, F., Hüneke, T., Jäkel, E., Järvinen, E., Jurkat, T., Kanter, S., Kästner, U., Kenntner, M., Kesselmeier, J., Klimach, T., Knecht, M., Kohl, R., Kölling, T., Krämer, M., Krüger, M., Krisna, T. C., Lavric, J. V., Longo, K., Mahnke, C., Manzi, A. O., Mayer, B., Mertes, S., Minikin, A., Molleker, S., Münch, S., Nillius, B., Pfeilsticker, K., Pöhlker, C., Roiger, A. E., Rose, D., Rosenow, D., Sauer, D., Schnaiter, M., Schneider, J., Schulz, C., de Souza, R. A. F., Spanu, A., Stock, P., Vila, D., Voigt, C., Walser, A., Walter, D., Weigel, R., Weinzierl, B., Werner, R., Yamasoe, M. A., Ziereis, H., Zinner, T., and Zöger, M.: The ACRIDICON-CHUVA campaign: Studying tropical deep convective clouds and precipitation over Amazonia using the new German research aircraft HALO, Bull. Am. Meteorol. Soc., doi:10.1175/BAMS-D-14-00255.1, 2016.

Wiensz, J. T., Degenstein, D. A., Lloyd, N. D., and Bourassa, A. E.: Retrieval of subvisual cirrus cloud optical thickness from limb-scatter measurements, Atmos. Meas. Tech., 6, 105–119, doi:10.5194/amt-6-105-2013, 2013.

Winker, D. M. and Trepte, C. R.: Laminar cirrus observed near the tropical tropopause by LITE, Geophys. Res. Lett., 25, 3351–3354, 1998.

Wirth, M., Fix, A., Mahnke, P., Schwarzer, H., Schrandt, F., and Ehret, G.: The airborne multi-wavelength water vapor differential absorption lidar WALES: System design and performance, Applied Physics B-Lasers And Optics, 96, 201–213, 2009.

Woodbury, G. E. and McCormick, M. P.: Zonal and geographical distributions of cirrus clouds determined from SAGE data, J. Geophys. Res. Atmos., 91, 2775–2785, doi:10.1029/JD091iD02p02775, 1986.

Yang, H. Y., Dobbie, S., Herbert, R., Connolly, P., Gallagher, M., Ghosh, S., Al-Jumur, S. M. R. K., and Clayton, J.: The effect of oberserved vertical structure, habits, and size distribution on the solar radiative properties and cloud evolution of cirrus clouds, Quart. J. R. Met. Soc., 138, 1221–1232, 2012.

Yang, P., Bi, L., Baum, B. A., Liou, K. N., Kattawar, G. W., Mishchenko, M. I., and Cole, B.: Spectrall consistent scatterin, absorption, and polarization properties of atmospheric ice crystals at wavelengths from 0.2 to 100 μm, J. Atmos. Sci., 70, 330–347, 2013.

Zhang, Y., Macke, A., and Albers, F.: Effect of crystal size spectrum and crystal shape on stratiform cirrus radiative forcing, Atmos. Res., 52, 59–75, 1999.

We thank the reviewer for the encouraging words and fort he helpful comments which improved the manuscript noticeably. By adding some more explanations and hints from a person not involved in the manuscript preparation enhanced the understanding for the reader.

The replies of the reviewer comments are given in the following manner: Reviewer comments are printed in bold, are labeled, and are listed in the beginning of each answer. The reviewer comments are followed by the author comments and revised parts of the paper. The revised parts of the paper are written in quotation marks and italic letters.

Comments:

1. **In general, I don't see a clear connection between the sensitivity analysis presented in Section 2 and the results and discussion presented in Section 4. Some paragraphs or Sentences explicitly linking the two sections where necessary would be appropriate.**

   The reviewer is right, the connection between the sensitivity study and the application to airborne measurements was not exactly pointed out. This might have been caused by relative high optical thickness of the cirrus selected for the case study. The choice of this case is now justified in the manuscript. The cirrus ranges in the range of $\tau < 1$ where sideward viewing observations are more sensitive compared to nadir observations. The following passages have been added and linking sentences and references were added to the corresponding sections 2 and 4 to show the linkage between simulations and measurements. Additional, in several parts of Section 4 and 5 the revised manuscript now refers to the results of the sensitivity study and highlights the differences between the two viewing geometries.

   "The RTS suggest that sideward viewing observations at near IR wavelengths ($\lambda > 900$ nm) are more suitable for the detection of SVC and cirrus. As a result the retrieval in Section 4 is performed at 1180 nm and 1600 nm wavelength in the IR region which are sensitive to tau and reff and not disturbed by Rayleigh scattering."

   "Considering these findings, the retrieval of tau in Section 4 is performed for $\Theta_V <= 60°$ only."

   "The sensitivity studies in Section 2.4 suggest that a combination of nadir and sideward viewing measurements allow a retrieval of tau for wide range of cirrus clouds depending on the observation conditions. For thin clouds the sideward viewing geometry would be preferred. In case the cloud becomes optically too thick, leading to high upward $I^V_{S,1180}$ and a saturation of ε_τ, no retrievals of tau are possible. Then, switching to nadir observations of $I^N_{S,1180}$ still enables to determine the amount of reflected radiation and to retrieve τ."

   "Referring to the sensitivity studies from Section 2 the influence of alpha and the ice crystal shape effects on the upward I measured in nadir geometry is larger compared to the sideward viewing measurements. While nadir observations, especially of optical thin clouds, are strongly influenced by α, sideward viewing observations are less effected. This is demonstrated in this case study where the sea surface albedo may vary due to different

surface wind speeds (Cox and Munk, 1954) and indicates the advantage of sideward viewing measurements."

"The retrieval using mini-DOAS sideward channels is also successful demonstrated for a reduced set of observations limited to Θ_V between 85° and 90°. Differences in τ range up to +-0.73 between SMART and mini-DOAS sideward viewing observations and are partly caused by the different viewing geometries. First, the sideward telescopes view into starboard direction, probing the cirrus cloud top at approximately 8000 m aside the flight track. Second, the nadir observations may suffer from uncertainties in α while the sideward observations are less effected by changes in α. Even for sea surfaces as presented here, alpha may change due to different wind speeds. Other potential reasons are the assumed ice crystal shapes in the RTS and different field-of-view of the passive and active remote sensing instruments. This conclusion is apparent from different probability distributions. While SMART and mini-DOAS show a median around τ=0.4, the median for WALES is shifted to lower τ around 0.2, indicating that WALES observed small τ more frequently. The difference of mean values of τ between mini-DOAS sideward channels and WALES is smaller with +-0.05 (15.6%). This shows the advantage of the sideward viewing retrieval due to a reduced surface influence and lower retrieval uncertainty, because of high ε_τ compared to the nadir measurements."

2. **Abstract, lines 17-18. The simulations indicate that off-nadir measurements are more adequate to retrieve _ of thin clouds, but that is not observed in the retrievals from the aircraft measurements presented here (at least in the way they are currently presented). Please, rephrase.**

This is right, in the original manuscript the focus of the discussion was more on the discrepancy between nadir and WALES measurements rather than highlighting the good agreement of sideward viewing observations and WALES. In the revised manuscript, the view of the reader is now more shifted to this good agreement, what indeed reflects the results from the sensitivity study:
"The mean τ inferred from the mini-DOAS sideward viewing observations is significantly lower than measured by SMART and mini-DOAS nadir measurements. Differences in τ range up to +-0.73 between SMART and mini-DOAS sideward viewing observations. This may result from the different FOV of the sideward viewing geometry that does not observe the exact same clouds as SMART and nadir channels did. With the scanning sensors orientated to starboard the sideward viewing retrieval corresponds to cirrus 8 km east of the flight track. As the MODIS satellite image in Fig. 12 indicates, the cirrus becomes slightly thinner towards east, which possibly is due to the lower values of τ. Other potential reasons are the assumed ice crystal shapes for the RTS and different field-of-view of the passive and active remote sensing instruments. On the other hand, the agreement between mini-DOAS sideward observations and WALES is significantly better. The maximum difference of τ between mini-DOAS sideward channels and WALES is +-0.25 while the difference between the mean values is +-0.05 (15.6%). With WALES and mini-DOAS measuring in different viewing geometries but showing better agreement, the differences of τ retrieved by SMART is most likely caused by uncertainties in α. As discussed in Section 2.3, nadir observations are stronger affected by α

*than sideward observations. This is confirmed by the smaller differences between WALES and mini-DOAS sideward observations and indicates the advantage of the sideward viewing retrieval due to a reduced surface influence and lower retrieval uncertainty.***"**

*"As indicated in 14 (b) retrieved τ from WALES and the mini-DOAS sideward viewing channels agree well confirmed by the linear regression in Fig. 14 (c) that gives a slope of f(x) = 1.0328 * x close to unity. The overestimation of retrieved τ by the mini-DOAS nadir channels compared to the sideward channels is visible in Fig. 14 (d) which results in a linear fit of f(x) = 1.642 * x."*

3. **Page 2, line 19. "better quantify" instead of "quantify better". It is not clear what you mean by "appear worthwhile", rephrase.**

"In order to quantify the microphysical and optical properties of SVC, which are needed to determine their radiative effects, more observations of this cloud type are required."

4. **Page 3, line 1. Add a comma after "relevant parameters"**

Comma was added

5. **Page 3, line 5. Elaborate more the statement "As a result, airborne remote sensing is required to bridge local in-situ and global satellite observations."**

We rephrased this section to point out the relevance of airborne measurements in comparison to satellite and ground based observations.
"*While satellite observations are suited to study the global coverage of cirrus, their spatial and temporal resolution is still limited and can not resolve the high spatial variability of cirrus. As a consequence the 3-D radiative effects of different cirrus properties, e.g., tau, ice crystal size and shape, can not be studied using the coarse resolution of satellite remote sensing. Ground-based lidar and radar remote sensing can provide a high temporal resolution but are limited to a fixed location. In-situ airborne measurements can provide cirrus properties with both.***"**

6. **Page 3, line 20: "and are not routinely be used in trace gas measurements" is not clear. Please, rephrase.**

This was a wrong formulation of the sentence. The opposite is the case. We rephrased to:
"Since then, several applications based on this method were developed and are routinely be used, e.g. for trace gas measurements (Abrams et al., 1996; Wang et al., 1996; Clerbaux et al., 2003; Bourassa et al., 2005; Fu et al., 2007)."

7. **Page 5, line 5. The use of the acronym SZA and the symbol _0 for the solar zenith angle is redundant. Remove the acronym.**

The acronym was replaced by the symbol.

8. **Page 6, figure 2. In the lower part of the figure it will be more convenient to plot the relative differences normalized to the Radiance. That will help with the corresponding discussion in lines 13-16. Also, some text is missing in the figure caption.**

   The reviewer is right. Using the relative instead of the absolute differences in radiance makes the difference more clear. We, therefore, changed the plot according to the reviewers suggestion. The caption was extended.

9. **Page 6, line 3. Replace "wavelengths less. " by "wavelengths lower…"**

   Replaced.

10. **"The RTS suggest that off-nadir observations at near infrared wavelengths (λ > 900 nm) are more suitable for the detection of SVC and cirrus."**

    Sentence is replaced by the reviewers comment.

11. **Page 8, figure 4 and lines 9-13. Because of the different values of I under the different constraints you should consider providing the sensitivity in percentages.**

    Each panel in Figure 4 was calculated for a cirrus of fixed optical thickness. Therefore, using percentages instead of absolute values would not change the presentation and only scale the values. As the plots also aim to compare the four independent cases of different τ and Θ_0, we prefer to stick with the absolute units in order to allow such a comparison. A normalization of the individual cases would remove this information. However, to improve the readability of the plot, we changed the illustration to 1d plots instead of the original color-coded 2d plots. This will make a comparison of the values between the panels easier.

12. **Page 9, line 2. Do you mean "thick clouds, for larger optical thickness…" here?**

    Sentence has been changed.
    "While sideward viewing measurements are predicted to become saturated for thick clouds, for low tau the optimal Θ_V is about $\Theta_V = 60°$ with the largest ε_τ occurring for φ between 0° and 60°."

13. **Page 9, line 13. Remove "especially"**

    Removed.

14. **Page 9, line 25. You should consider include a plot with the steepest derivative (maybe a subplot in Figure 5?)**

We are not sure, what the reviewer exactly meant by this comment. Figure 5 show the linear increase of the measured upward radiance caused by an increase of the surface albedo. In all cases, the increase is almost linear and, therefore, no steepest derivative exists. Only for each case one derivative can be calculated and is given in Table 1.

15. **Page 11, figure 6. Please, include a subplot with the relative differences between the different ice crystals. This will help with the discussion in lines 8-13.**

We agree, that relative differences will enhance the illustration of the differences between simulations with different ice crystal shapes and added such as subplot.

16. **Page 12, line 6. "were investigated"**

Changed.
"…mid-latitudes were investigated in March and April…"

17. **Page 12, line 11. Provide references for SMART and the calibration procedure.**

The SMART instrument characteristics and the calibration procedure are given in Section 3.1. So we think there is no need to give additional reference about the calibration here. Here we only added a reference introducing SMART in general.
Wendisch, M., Müller, D., Schell, D., and Heintzenberg, J.: An airborne spectral albedometer with active horizontal stabilization, J. Atmos. Oceanic Technol., 18, 1856–1866, 2001

18. **Page 12, line13-14. Provide references for the mini-DOAS and the DOAS technique.**

The DOAS instrument characteristics and the DOAS technique are discussed in Section 3.2. Here we only added a reference introducing the mini-DOAS in general.
Hüneke, T.: The scaling method applied to HALO measurements: Inferring absolute trace gas concentrations from airborne limb spectroscopy under all sky conditions, Ph.D. thesis, Ruperto-Carola University of Heidelberg, Germany, 2016.

19. **Page 13, line 21. The symbol ILmD has not been defined before. Please, define.**

Thanks for finding this shortcoming. ILmD is the upward radiance measured by the mini-DOAS in off-nadir direction. We rephrased to:
"…applies least square retrievals on the spectral shape of the observed upward radiance ILmD by the mini-DOAS in sideward orientation…"

20. **Page 14, line 26. Why are multiple scattering effects neglected?**

Multiple scattering effects are not neglected. This impression might have come up due to the unclear wording. As the apparent transmission is not needed to understand the lidar method, we deleted this statement.
"Best compensation of the multiple scattering decay below the cloud is found for r_{eff} = 35+- µm in good agreement with the climatological values proposed by Bozzo_2008. The mean correction factor for the data set shown in this paper was 7%."

21. Page 16, Figure 8. Can you add the error bars to the plots? Especially to plots b and d. Idem for figure 9.

The uncertainty range has been added by shaded areas in both figures.

22. Page 19, lines 26-27. Please, elaborate the statement "These stop criteria determine the accuracy of the iterative retrieval."

We tried to rephrase the statement and added explanations to illustrate the iteration process better.
"The iteration of tau is repeated until the change of τ_n between two iteration steps is smaller than 5% or a limit of n>100 iteration steps is reached. These stop criteria determine the accuracy of the iterative retrieval. If a lower relative stop criteria (change of τ_n smaller than 5% between two iteration steps or more then 100 iteration steps) is used the iteration may come closer to the true searched value and the retrieval accuracy increases as well as the necessary iteration steps and the computational time. To limit the computational time, the second stop criteria is used to limit the maximum number of iteration steps."

23. Page 20, lines 1-15. What happens for off-nadir observations?

Right, we missed to add the same analysis for the retrieval using the sideward observations. In the revised version these information are added and emphasize the benefits of the sideward measurements:
"Simulations show, that for τ = 0.5 the difference of $I^N_{RTS,1600}$ in nadir direction is only 0.1 mW when changing r_eff from 10 µm to 20 µm indicating the low sensitivity of r_eff retrievals at this wavelength. Therefore, a reliable retrieval of r_eff with reasonable accuracy is not feasible. For $I^V_{RTS,1600}$ the difference is 1.4 mW m^{-2} sr^{-1} and about a magnitude larger indicating that a retrieval of r_eff might be reasonable. However, in order to be consistent between both nadir and sideward viewing retrieval, r_eff has been fixed. A value of r_eff = 30 µm was chosen, a typical value of ice crystals observed by in-situ measurements during ML-CIRRUS Voigt et al., 2016. Therefore, the influence of an invalid assumption of r_eff on the iterative retrieval is analyzed. For this purpose the retrieval is tested for a typical cirrus of τ=0.3 and is run with three different assumptions of r_eff of 20 µm, 30 µm, 40 µm, representing the uncertainty of r_eff. These simulations imply that the retrieved tau changes only by +-0.02 between smallest and largest r_eff, resulting in a relative error in τ of 6.7%. The uncertainty in measured $I^N_{RTS,1600}$ and $I^V_{md,1600}$ causes a retrieval uncertainty of less than τ= +- 0.2. This justifies the fixed choice of r_eff in this specific cloud case."

24. Page 21, Figure 12. Axis labels are missing.

Labels are added to the plot.

25. Page 22, lines 14-15. Are these average values obtained for the coincident measurements only? Otherwise, comparing the different values is not realistic. Especially for the DOAS off-nadir, which have a smaller temporal resolution and does not capture all the variability observed during the analyzed period.

The reviewer is right and the method to calculate the averages is now included in the manuscript.
"Average τ are calculated for the filtered time period (indicated by the grey box in Fig. 14 for each instrument. Due to different sampling intervals, a different resolution and number of observations are included in the averaging calculations."

26. Page 23, line 3. A more in-depth analysis of the uncertainty will be useful, mainly for inter-comparison purposes between the different datasets presented in figure 14.

More detailed explanation of the error estimation is added.
"The uncertainty range of tau is determined by running the retrieval twice with a bias of measured $I^N_{S,1180}$ with +-14.5% uncertainty at 1180 nm wavelength as upper and lower border. The resulting upper and lower retrieved tau represent the retrieval uncertainty."

27. Page 23, line 9 and figure 14. It looks like there is a better agreement between the DOAS off-nadir and the reference WALES than between the DOAS off-nadir and DOAS nadir or SMART. Can you comment something on that? Can you further discuss the advantages and disadvantages of having nadir and off-nadir measurements and link it with the sensitivity analysis in section 2?

Resulting from the different observation geometries of the nadir looking sensors and the mini-DOAS sideward sensors different cloud scenes are probed. This can lead to the different values of retrieved tau and the good agreement between mini-DOAS sideward and WALES. Please have a look to the added description.
"Average τ are calculated for the filtered time period (indicated by the grey box in Fig. 14 for each instrument. Due to different sampling intervals, a different resolution and number of observations are included in the averaging calculations. The retrieved average of τ at 532 nm is 0.54+-0.2 (SMART), 0.49+-0.2 (mini-DOAS nadir spectrometer), 0.27+-0.2 (mini-DOAS sideward viewing spectrometer) and 0.32+-0.02 (WALES). The results indicate a reasonable agreement of τ retrieved by SMART and mini-DOAS nadir channel, while lower τ are inferred from mini-DOAS sideward viewing and WALES measurements. Taking the WALES measurements as a reference, the measurements of SMART and mini-DOAS overestimate τ. However, by estimating the uncertainty of the mini-DOAS and SMART basing on RTS, the measurement error of $I^N_{S,1180}$ (14.5%) by SMART results in an uncertainty range of retrieved τof +-0.2, which covers the values of τobtained by WALES. The uncertainty range of τis determined by running the retrieval twice with a bias of measured $I^N_{S,1180}$ with +-14.5%

uncertainty at 1180 nm wavelength as upper and lower border. The resulting upper and lower retrieved τ represent the retrieval uncertainty. The mean τ inferred from the mini-DOAS sideward viewing observations is significantly lower than measured by SMART and mini-DOAS nadir measurements. Differences in τ range up to +-0.73 between SMART and mini-DOAS sideward viewing observations. This may result from the different FOV of the sideward viewing geometry that does not observe the exact same clouds as SMART and nadir channels did. With the scanning sensors orientated to starboard the sideward viewing retrieval corresponds to cirrus 8 km east of the flight track. As the MODIS satellite image in Fig. 12 indicates, the cirrus becomes slightly thinner towards east, which possibly is due to the lower values of τ. Other potential reasons are the assumed ice crystal shapes for the RTS and different field-of-view of the passive and active remote sensing instruments. On the other hand, the agreement between mini-DOAS sideward observations and WALES is significantly better. The maximum difference of τ between mini-DOAS sideward channels and WALES is +-0.25 while the difference between the mean values is +-0.05 (15.6%). With WALES and mini-DOAS measuring in different viewing geometries but showing better agreement, the differences of τ retrieved by SMART is most likely caused by uncertainties in α. As discussed in Section 2.3, nadir observations are stronger affected by α than sideward observations. This is confirmed by the smaller differences between WALES and mini-DOAS sideward observations and indicates the advantage of the sideward viewing retrieval due to a reduced surface influence and lower retrieval uncertainty."

28. Page 23, lines 20-21. This statement is not clear. If the data points contaminated by the second cloud layer are excluded from the calculations, what do you mean here?

This statement was misleading. The section of the time series used to calculate the average values was carefully selected for an area where no second cloud layer was observed. This selection bases on the analysis of the WALES profiles. However, due to the larger FOV of the passive sensors, there is the chance that SMART and mini-DOAS are still contaminated by such a second cloud layer but not WALES. We extended the description of the data selection for the calculation of the averages.
All points which differed clearly were excluded from the calculations. Nevertheless there is a slight chance that few points were classified as cirrus but actually belong to the second cloud layer. This is mostly due to the fact that they could not be separated definitely and because the SMART and mini-DOAS sensors have a larger FOV compared to WALES.
"…These data points are excluded from the following analysis. Nevertheless there is a slight chance that few points were classified as cirrus but actually belong to the second cloud layer. This is mostly due to the fact that they could not be separated definitely and because the SMART and mini-DOAS sensors have a larger FOV compared to WALES."

29. Page 24, lines 10-12. This is not clear either. From the results and the discussion presented before, it looked like you were using the wavelength of 532 nm for all the instruments. Please, clarify where necessary.

The reviewer is right, this statement might be misleading. The measurements of the different sensors have been analyzed at different wavelengths (1180 nm for SMART and

mini-DOAS and 532 nm for WALES). However, the retrieved cirrus optical thickness always refers to 532 nm. Therefore, the retrieval for the passive remote sensing of SMART and mini-DOAS consider simulations at both wavelengths. In the radiative transfer simulations the cirrus optical thickness is defined and changed at 532 nm while the simulations and measurements at 1180 nm were compared to find the correct solution:
"Additionally, the different wavelengths of the measurements may introduce biases in the retrieved tau due to different penetration depth of the reflected radiation into the cloud (Platnick, 2000). Therefore, the wavelength selection defines the layer in the cloud which is probed. While WALES uses backscatter measurements at lambda= 532 nm and lambda= 1064 nm the measurements of $I_{S,1180}$ by SMART and mini-DOAS are performed at τ= 1180 nm. Although the retrieval accounts for the wavelength dependence of scattering, absorption and refraction on ice crystals (Takano and Liou, 1989; Yang et al., 2013) by scaling the retrieved tau at λ = 1180 nm to λ= 532 nm to make it comparable between the instruments."
"The retrieval of tau by SMART and mini-DOAS bases on the measurements at λ = 1180 nm and is scaled to λ = 532 nm to consider the wavelength dependence of tau and to be able to compare it with WALES measurement at λ = 532 nm. Therefore, the retrieval considers RTS at both wavelengths. In the RTS τ is defined and changed at λ = 532 nm while the measurements are compared to simulations at λ = 1180 nm to determine the correct solution."

30. Page 26, line 14. Agreement is within the uncertainty but I would not consider a 66.6Numerical values for the differences between DOAS nadir and Wales and DOAS off-nadir should be included separately. Relevance was given to the comparison between the nadir and off- nadir observations in the sensitivity analysis and it will be interesting to do a clear distinction also for the in-situ airborne data and include a significant conclusion at this respect.

To add an explicit comparison of the DOAS sideward and nadir results we added an additional 1:1 plot in Figure 15. Here the calculated mean optical thickness values have to be analyzed as done in section 5.2.1. Alternatively, we show a comparison between DOAS-sideward and WALES measurements in the additional 1:1 plot. A good agreement was found indicating also that DOAS-sideward and DOAS-nadir will have an agreement similar to the comparison of WALES and DOAS-nadir. This illustrates the capability of sideward measurements to observe optically thin cirrus and the higher accuracy of this method for optical thin clouds. There conclusions have been added.

We thank the reviewer for the encouraging words and fort he helpful comments which improved the manuscript noticeably. By adding some more explanations and hints from a person not involved in the manuscript preparation enhanced the understanding for the reader.

The replies of the reviewer comments are given in the following manner: Reviewer comments are printed in bold, are labeled, and are listed in the beginning of each answer. The reviewer comments are followed by the author comments and revised parts of the paper. The revised parts of the paper are written in quotation marks and italic letters.

Comments:

1. **Page 2: there are significant discussions for SVC, but techniques presented here a not suitable for dealing with cirrus with such small optical depth- large uncertainties among them.**
   The reviewer is right. In the manuscript a case study of an observed cirrus with higher optical thickness than SVC is presented. However, the sensitivity study (Figure 3) shows that the sensitivity of measured radiance is higher for sideward measurements compared to nadir measurements for cirrus with low optical thickness up to τ=1. The observed cirrus case showed τ in the range of 0.2-1.0 and, therefore, is suitable to test the different observation geometries although it is not in the range of SVC. Using a cirrus with higher optical thickness than SVC as a first test case has the advantage, that the measurement uncertainties are less important for the retrieved τ (higher reflected radiance way above the instrument noise level). Therefore, we think that using a moderate thick cirrus is most suited here. Additionally, Sections 4 and 5 (especially 5.2.1) include a more detailed investigation of the mini-DOAS sideward observations, indicating and emphasizing the advantages of these observations compared to measurements in nadir geometry for all types of thin cirrus clouds including SVC. Furthermore two plots were added to Figure 15 to show the agreement of tau between WALES and the mini-DOAS sideward measurements.

   "The retrieval using mini-DOAS sideward channels is also successful demonstrated for a reduced set of observations limited to Θ_V between 85° and 90°. Differences in τ range up to +-0.73 between SMART and mini-DOAS sideward viewing observations and are partly caused by the different viewing geometries. First, the sideward telescopes view into starboard direction, probing the cirrus cloud top at approximately 8000 m aside the flight track. Second, the nadir observations may suffer from uncertainties in α while the sideward observations are less effected by changes in α. Even for sea surfaces as presented here, αmay change due to different wind speeds. Other potential reasons are the assumed ice crystal shapes in the RTS and different field-of-view of the passive and active remote sensing instruments. This conclusion is apparent from different probability distributions. While SMART and mini-DOAS show a median around τ=0.4, the median for WALES is shifted to lower τ around 0.2, indicating that WALES observed small τ more frequently. The difference of mean values of τ between mini-DOAS sideward channels and WALES is smaller with +-0.05 (15.6%). This shows the advantage of the sideward viewing retrieval due to a reduced surface influence and lower retrieval uncertainty, because of high ε_τ compared to the nadir measurements."

2. **Page 2, last sentenceâ˘A ˇ Tit is not an accurate statement if you consider passive sensor measurements.**
   Sentence is rephrased and the word "inherently" is removed.
   "While satellite observations are suited to study the global coverage of cirrus, their spatial and temporal resolution is still limited and can not resolve the high spatial variability of cirrus."

3. **Page 3: Lines 5-6: the cirrus optical thickness of water clouds does not make senseâ˘A ˇTre-write.**
   The word "cirrus" is removed from the sentence as water clouds can not be cirrus.
   "For nadir measurements tau and the effective radius r_eff of liquid water droplets can be retrieved by the bi-spectral reflectivity method after Twomey, 1980 and Nakajima, 1990. Ou et al., 1993, Rolland et al. 2000, and King et al., 2004 adapted this method for ice clouds by introducing some modifications with regard to the thermodynamic phase and crystal shape of the ice particles."

4. **Page 4: Line 18: If you conclude that it is impossible here. You don't need any further study in this paper. Yes, it is challenging, which indicates that we need more observational constrains to improve the retrieval.**
   This statement did not ment that cirrus retrieval are in general impossible. "Impossible" referred to the worst conditions where uncertainties may get too large. Most observations will provide conditions where a retrieval is possible but with uncertainties. Therefore, the conclusion was rewritten:
   "In a worst scenario, all these effects render retrievals of τ to become rather inaccurate. However, observations in sideward or limb viewing direction and improvements of retrieval techniques may overcome these limitations."

5. **Page 4, Lines 19-21: The statements here are not accurate. Off-nadir measurements are widely used for space-base cirrus remote sensing. As you know, most satellite passive sensors are wide swath measurements .**
   That is correct. Sideward can mean 1° off-nadir viewing direction. With "sideward" we address measurements close to limb direction (90° viewing direction). We refrain of using the term "limb" measurements because the measurements presented in the manuscript had been performed at viewing angles less than 90°, not limb. We now included an explanation on what we define as sideward measurements and in case literature is discussed where real limb-measurements are applied, we now kept writing limb viewing angle. The word "off-nadir" was replaced by "sideward" in the entire manuscript to avoid misunderstanding.
   "Limb measurements of SVC and cirrus were first introduced and utilized for satellite measurements by Woodbury, 1986. Since then, several applications based on this method were developed and are routinely be used, e.g. for trace gas measurements (Abrams_1996, Wang_1996, Clerbaux_2003, Bourassa_2005, Fu_2007).
   Many trace gas retrievals from aircraft, balloons and satellites are based on ultraviolet (UV)/ visible (VIS)/ near infrared (IR) sideward viewing measurements in combination with

differential optical absorption spectroscopy (DOAS), e.g. performed by Platt_2008. Compared to nadir observations, radiance measurements in limb or sideward viewing geometry are supposed to be more sensitive to optical thin clouds due to their observation geometry. One recent study was accomplished by Wiensz 2013 who used satellite limb measurements especially for SVC investigation in the tropical tropopause layer. This data source improved SVC observations with respect to cloud climatology and microphysics."

6. **Page 4, Line 25, "highly sensitive": An overstatement. Yes, it is more sensitive, but it is highly dependent on the magnitude of off-angle.**
   Replaced the word "highly" by "more" to avoid the overstatement. The influence of the observation angle is shown later in the different simulations of the sensitivity study.
   "Compared to nadir observations, radiance measurements in limb or sideward geometry are supposed to be more sensitive to optical thin clouds due to their observation geometry."

7. **Page 5, Line 15: What does "F" in "FDISORT" mean?**
   FDISORT is the Fortran 77 version of the original DISORT solver:
   "*The Fortran 77 discrete ordinate radiative transfer solver version 2.0 (FDISORT 2) after Stamnes 2000 is chosen.*"

8. **Page 6: Figure 2 caption in the PDF misses words.**
   Caption is corrected.

9. **Page 6, line 15: The statement of "cirrus can not be detected" is not accurate. Cirrus is a general category including high clouds with optical depth up to 3.**
   Sentence is formulated more precisely just refereeing to sub visible cirrus:
   "*Therefore, at λ= 532 nm SVC with τ= 0.03 which is presented in the simulations can not be detected.*"

10. **Page 7, lines 4-5: To draw this conclusion, you'd better to present calculation results with a higher optical depth.**
    Thanks for this suggestion. We added simulations for a cirrus with τ=2.0 in the revised manuscript what helped to illustrate the differences to the SVC case. The simulations for τ=2.0 show that the effect of Rayleigh scattering is significant reduced at 532 nm and a separation between cloudy and clear-sky is possible for such clouds. Nevertheless, the relative difference between cloudy and clear-sky case is still more pronounced for the radiance at 1180 nm and emphasizes the conclusion:
    "For comparison, simulations of a thicker cirrus with τ= 2.0 are presented in Figure 2 (b). Here, the influence of the Rayleigh scattering at λ= 532 nm is reduced and a distinction between cloudy and clear-sky conditions becomes possible. However, the relative difference between cloudy and clear-sky is still more pronounced at λ= 1180 nm.
    The RTS suggest that sideward viewing observations at near IR wavelengths (λ> 900 nm) are more suitable for the detection of SVC and cirrus. As a result the retrieval in Section 4 is performed at 1180 nm and 1600 nm wavelength in the IR region which are sensitive to τand r_eff and not disturbed by Rayleigh scattering."

11. **Page 7, line 15: This statement does not consistent with the statements in the next paragraph.**

    Statement was rephrased and specified for cirrus with optical thickness below 1. It was added that for clouds with optical thickness larger than 1 the sensitivity of sideward observations is in the same range compared to nadir measurements. This shows that sideward measurements are most suited and applicable for cirrus with tau below 1.
    "Due to the apparent longer LOS for both Θ_0, sideward viewing sensor orientations yield larger ε_τ of simulated I^V_{RTS} as compared to the nadir geometry for cirrus clouds with $\tau<1$ which includes SVC. This indicates that sideward measurements are most suited to retrieve tau below 1 and for the detection of SVC. The almost linear increase of the nadir radiance I^N_{RTS} indicates a constant ε_τ tau for the investigated range of tau and Θ_0. For $\tau >= 1$ the sensitivity of sideward viewing observations is in the same range compared to nadir measurements or slightly lower depending on the combination of Θ_0 and Θ_V."

12. **Page 8, line 1-2: To draw this conclusion, you need to make many assumptions.**

    Conclusion is extended and explained in more detail.
    "For low tau and a high sun, the highest ε_τ is given for the sideward viewing geometry (Θ_V = 78°) for $\tau <= 1$. A similar pattern emerges for low Sun (Θ_0 = 75°) resulting in larger ε_τ and a steep decrease for increasing τ. It shows that ε_τ decreases with tau and for $\tau < 2$ drops below ε_τ of nadir measurements. The sensitivity of I with respect to τ can also be interpreted in terms of the uncertainty of retrieved τ related to an initial uncertainty in measured I. The higher ε the weaker the impact of uncertainties in the measurements on the uncertainties of the retrieved τ. As shown in Fig.3 (b), a high ε_τ is calculated for $I_{RTS,1180}$ for $\tau <= 1$ and indicates a lower measurement uncertainty. Therefore, sideward viewing observations at λ= 1180 nm allow a more accurate determination of τ compared to nadir observations for optical thin clouds with $\tau <= 1$."

13. **Page 8, line 7: Based on the statement, it seems that you don't consider angle smaller than 60 degree as the off-nadir observations. That is not right.**

    See reply to comment 5.
    Sideward measurements with angles smaller than 60 degree are not that sensitive as compared to larger angles. This does not necessarily mean that they are not considered but they are unfavorable. The plot should show that depending in the optical thickness and the relative solar azimuth angle the best viewing angle should be selected to reach the highest sensitivity which results in the lowest relative measurement errors and better retrieval results.
    "For τ= 0.1 and Θ_0= 25°$ (Fig. 4 a), ε_τ ranges between 5 and 66 mW m^{-2} nm^{-1} sr^{-1}. For larger Θ_V (sideward viewing observations) ε_τ increases significantly reaching the maximum for Θ_V =90° and φ = 0°. Observations under these angles are better suited in comparison to other angle combinations as they enable to achieve the largest possible ε_τ and reduced relative measurement errors which results in increased retrieval accuracy."

14. **Page 9, line 9-10: It is hard to understand this sentence.**

In the revised manuscript we rephrased the sentence:
"Measurements in sideward viewing geometry strongly dependent on Θ_V especially around Θ_V = 90°. In order to avoid spurious results by mispointing with the sensor, a careful alignment of the optical sensor and an accurate determination is required. Considering these findings, the retrieval of tau in Section 4 is performed for Θ_V <= 60° only."

15. **Page 12, figure 7: It is hard to see the location of the optical port in (b). A better figure may be needed.**
    Location of the ports is highlighted in an updated figure and is hopefully visible now.

16. **Page 12, line 12: UV and VIS were defined early.**
    Removed.

17. **Page 12, line 13: DOAS was defined early. –Avoid multiple definitions.**
    Removed.

18. **Page 15, line 3: "cross-calibrate both instrument" is no right. As you discussed in the paper, SMART is lab calibrated.**
    The sentence was rephrased:
    "*Since no radiometric calibration is available for mini-DOAS, simultaneous measurements of SMART and mini-DOAS are used to cross-calibrate the mini-DOAS with SMART.*"

19. **Page 16, lines 1-2: Giving absolute numbers are needed, but it will be good to present relative differences too.**
    We added relative differences for the nadir and sideward cross-calibration in the revised text.
    "…, which results in relative differences of 5.4% at λ= 1180 nm and 1.9% at λ= 1600 nm compared to the SMART absolute values."

20. **Page 18, line 3: Based on Fig. 10, I'd like to say that 2.9 is a big number, which is difficult to support the stable calibration consistent.**
    Yes, 2.9 actually is a big number considering the aim to retrieve cirrus optical thickness with reasonable accuracy. We, therefore, included estimates of uncertainties in the retrieval of tau that would be caused by such uncertainties in the calibration.
    However, the comparison of the calibrations did not suggest to use a calibration that was done long before or after the measurements. This was now emphasized in the revised manuscript.
    Nevertheless, considering the original purpose of the mini-DOAS to remain a precise wavelength calibration for DOAS observations but without need to relying on a radiometric calibration because relative measurements are analyzed, the relative good stability of the calibration was surprising. The radiometric calibration can change between campaigns due to instrument removal and modification but also between flights by switching the instrument on and off. As the deviation is 2.9 and ranging in the uncertainty range of SMART the stability is good taking SMART as a reference. If no subsequent calibration of the mini-

DOAS would be available, radiometric measurements would still be possible considering the uncertainty of 2.9 mW, what may in some application be sufficient.

21. **Page 19, Line 26: The statement here is not consistent with the lowest box in Fig. 11.**
    Illustration is corrected so it is in agreement with the text.

22. **Page 20, line 20: Even for lidar guy, it is hard to see contrails in Fig. 13. How about to plot Fig. 13 as a color figure to make the fine feature easy to identify.**
    B/W-plot was replaced by a color plot.

23. **Page 22, line 22: For cirrus cloud optical depth around 1, it is hard to claim that the lower layer is obscured by the upper cloud layer. The lower layer can be clearly identified from lidar image.**
    This is correct. We did not clearly separate this discussion between lidar and passive sensors. Of course, the lidar can provide vertically resolved measurements and, therefore, is able to separate the second cloud layer. This means that WALES can determine tau of the cirrus (without the lower layer) correctly. On the other hand SMART provides only vertically integrated information as it measures the sum of reflected radiation from both clouds. This partly explains the bias in the retrieval. The paragraph was rephrased.
    "A second segment with higher retrieved τ is likely due to an underlying cirrus between 8.5 km and 9.5 km altitude that is also obscured to the detection by WALES. Therefore, a positive systematic offset of the retrieved τ occurs for SMART and mini-DOAS. These data points are excluded from the following analysis. Nevertheless, there is a slight chance that a few cloud fragments of these second cloud layers are still affecting the SMART- and mini-DOAS retrieval. Both passive sensors have a larger FOV compared to WALES and, therefore, are more likely sensitive to cloud layers located below the cirrus."

24. **Page 23, line 3: Is 10% here mean error or random error? You need to explain the +0.2 overestimation.**
    The measurement uncertainty of SMART is 14.5% and not 10%. This was corrected in the manuscript. The uncertainty of ±0.2 results from the uncertainty in the measured upward radiance of 14.5%. For this estimation the retrieval was performed twice with a bias of *I* with ±14.5% uncertainty as upper and lower border. We rephrased the paragraph to make this procedure more clear:
    "The uncertainty range of tau is determined by running the retrieval twice with a bias of measured $I^{N}_{S,1180}$ *with +-14.5% uncertainty at 1180 nm wavelength as upper and lower border. The resulting upper and lower retrieved tau represent the retrieval uncertainty."*

25. **Page 23, lines 16-23: Which kind of calibration errors explain the good linear correlations and 0.66 or 0.69 slopes?**
    SMART and mini-DOAS relay on a large field of view, in the range of several tenth of meters depending on the distance between sensor ans cloud top, compared to WALES which has a narrow opening angle of 0.08°. Additionally, SMART and mini-DOAS are passive remote

sensing instrument measureing the scattered radiation from the sun which is effected by the entire atmosphere. Contrarily, the WALES measurement is influenced by interactions in the smaller field of view only. Also the food print at cloud top is much smaller from WALES compared to SMART and mini-DOAS. Therefore, WALES has a higher horizontal resolution. This becomes visible in the propability density functions of the three instruments, where the median for WALES is shifted to lower optical thickness, indicating that WALES measured more values of low tau and even cloud free regions. On the other hand SMART and mini-DOAS measurements average over larger areas and do not represent these small fluctuations which can explain the linear offset.
Due to the larger FOV of the passive sensors, there is the chance that SMART and mini-DOAS are still contaminated by a second cloud layer but not WALES. We extended the description of the data selection for the calculation of the averages.
All points which differed clearly were excluded from the calculations. Nevertheless there is a slight chance that few points were classified as cirrus but actually belong to the second cloud layer. This is mostly due to the fact that they could not be separated definitely and because the SMART and mini-DOAS sensors have a larger FOV compared to WALES.

26. Page 24, lines 10-11: For large ice crystals, why do you expect optical depth difference between 532 nm and 1180 nm?

For the retrieval of optical thickness the wavelength applied in the retrieval has to be considered as the ice crystal extinction is wavelength dependent (Takano and Liou, 1989, Yang et al., 2012).
Although, this dependence was considered by scaling all results to lambda= 532 nm, the reflected radiance at different wavelengths used for the retrieval have different vertical weighting functions (Platnick, 2000). Depending on the wavelength, the penetration depth of solar radiation into a cloud can vary. While wavelengths close to the UV have a higher penetration depth compared to wavelength close to the infrared region.
This effect might be small in case of vertically homogeneous cirrus but is a potential uncertainty source which have to be considered for vertical inhomogeneous cirrus observed here.
"Additionally, the different wavelengths of the measurements may introduce biases in the retrieved tau due to different penetration depth of the reflected radiation into the cloud (Platnick, 2000). Therefore, the wavelength selection defines the layer in the cloud which is probed. While WALES uses backscatter measurements at λ= 532 nm and λ= 1064 nm the measurements of $I_{S,1180}$ by SMART and mini-DOAS are performed at λ= 1180 nm. Although the retrieval accounts for the wavelength dependence of scattering, absorption and refraction on ice crystals (Takano_1989,Yang_2013) by scaling the retrieved τ at λ= 1180 nm to λ = 532 nm to make it comparable between the different instruments."

Takano, Y. and K. Liou, 1989: Solar Radiative Transfer in Cirrus Clouds. Part I: Single-Scattering and Optical Properties of Hexagonal Ice Crystals. J. Atmos. Sci., 46, 3–19, doi: 10.1175/1520-0469(1989)046<0003:SRTICC>2.0.CO;2.

Yang, P., L. Bi, B. Baum, K. Liou, G. Kattawar, M. Mishchenko, and B. Cole, 2013: Spectrally Consistent Scattering, Absorption, and Polarization Properties of Atmospheric Ice Crystals at Wavelengths from 0.2 to 100 µm. J. Atmos. Sci., 70, 330–347, doi: 10.1175/JAS-D-12-039.1.

Platnick, S., 2000: Vertical photon transport in cloud remote sensing problems. J. Geophys. Res. Atmos., 105, 22919-22935, doi: 10.1029/2000JD900333.